Redox Biology 24 (2019) 101199

Contents lists available at ScienceDirect

Redox Biology

journal homepage: www.elsevier.com/locate/redox

Research Paper

Hyperhomocysteinemia-induced death of retinal ganglion cells: The role of Müller glial cells and NRF2

Soumya Navneet[a,b], Jing Zhao[b,c], Jing Wang[a,b], Barbara Mysona[a,b,c], Shannon Barwick[a,b], Navneet Ammal Kaidery[d,e], Alan Saul[b,c], Ismail Kaddour-Djebbar[h,i], Wendy B. Bollag[h,i], Bobby Thomas[d,e,f,g], Kathryn E. Bollinger[a,b,c], Sylvia B. Smith[a,b,c,*]

[a] Department of Cellular Biology and Anatomy, Medical College of Georgia, Augusta University, Augusta, GA, USA
[b] James and Jean Culver Vision Discovery Institute, Augusta University, Augusta, GA, USA
[c] Department of Ophthalmology, Medical College of Georgia, Augusta University, Augusta, GA, USA
[d] Department of Pharmacology and Toxicology, Medical College of Georgia, Augusta University, Augusta, GA, USA
[e] Department of Pediatrics, Medical University of South Carolina, Charleston, SC, USA
[f] Department of Neuroscience, Medical University of South Carolina, Charleston, SC, USA
[g] Department of Drug Discovery, Medical University of South Carolina, Charleston, SC, USA
[h] Department of Physiology, Medical College of Georgia, Augusta University, Augusta, GA, USA
[i] Charlie Norwood VA Medical Center, One Freedom Way, Augusta, GA, 30904, USA

ARTICLE INFO

Keywords:
Retina
Ganglion cells
Hyperhomocysteinemia
Cystathionine β-synthase
Methylene tetrahydrofolate reductase
Mouse
Glaucoma
Homocysteine
NRF2

ABSTRACT

Hyperhomocysteinemia (Hhcy), or increased levels of the excitatory amino acid homocysteine (Hcy), is implicated in glaucoma, a disease characterized by increased oxidative stress and loss of retinal ganglion cells (RGCs). Whether Hhcy is causative or merely a biomarker for RGC loss in glaucoma is unknown. Here we analyzed the role of NRF2, a master regulator of the antioxidant response, in Hhcy-induced RGC death *in vivo* and *in vitro*. By crossing *Nrf2*$^{-/-}$ mice and two mouse models of chronic Hhcy (*Cbs*$^{+/-}$ and *Mthfr*$^{+/-}$ mice), we generated *Cbs*$^{+/-}$*Nrf2*$^{-/-}$ and *Mthfr*$^{+/-}$*Nrf2*$^{-/-}$ mice and performed systematic analysis of retinal architecture and visual acuity followed by assessment of retinal morphometry and gliosis. We observed significant reduction of inner retinal layer thickness and reduced visual acuity in Hhcy mice lacking NRF2. These functional deficits were accompanied by fewer RGCs and increased gliosis. Given the key role of Müller glial cells in maintaining RGCs, we established an ex-vivo indirect co-culture system using primary RGCs and Müller cells. Hhcy-exposure decreased RGC viability, which was abrogated when cells were indirectly cultured with wildtype (WT) Müller cells, but not with *Nrf2*$^{-/-}$ Müller cells. Exposure of WT Müller cells to Hhcy yielded a robust mitochondrial and glycolytic response, which was not observed in *Nrf2*$^{-/-}$ Müller cells. Taken together, the *in vivo* and *in vitro* data suggest that deleterious effects of Hhcy on RGCs are likely dependent upon the health of retinal glial cells and the availability of an intact retinal antioxidant response mechanism.

1. Introduction

Homocysteine (Hcy) is a sulfur-containing amino acid that stands at the intersection of the remethylation and transsulfuration metabolic pathways. Pathological elevation of Hcy, termed hyperhomocysteinemia (Hhcy) is associated with cardiovascular diseases such as atherosclerosis and congestive heart failure, as well as neurodegenerative diseases such as dementia, Parkinson's and Alzheimer's disease [1,2]. Oxidative stress is a major pathogenic mechanism associated with Hhcy [3]. As the retina is a neurovascular tissue, it is not surprising that Hhcy has been implicated in retinal diseases including retinal vessel occlusive disease, optic atrophy, and macular degeneration [4]. There has been considerable interest in the role of Hhcy in various forms of glaucoma, a complex disease in which retinal ganglion cell (RGC) loss leads to severe visual impairment. Hhcy has been studied extensively in exfoliation syndrome (XFS) [5–7], the most common cause of open-angle glaucoma worldwide [8]. Hcy levels are elevated significantly in the aqueous humor, plasma, and tears of XFS patients, but questions remain as to whether Hcy is a “disease driver, disease biomarker or innocent bystander to some biochemical process related

* Corresponding author. Department of Cellular Biology and Anatomy, Medical College of Georgia, Augusta University, 1120 15th Street, CB 1114, Augusta, GA, 30912-2000, USA.
E-mail address: sbsmith@augusta.edu (S.B. Smith).

https://doi.org/10.1016/j.redox.2019.101199
Received 13 March 2019; Received in revised form 5 April 2019; Accepted 10 April 2019
Available online 11 April 2019

to Hcy metabolism" [9].

To understand the relationship between Hhcy and RGC survival, several *in vitro* and *in vivo* studies have been performed and reported. *In vitro* studies demonstrated that exposure of primary murine RGCs to moderate elevation of Hcy [50 μM] resulted in death of more than half of the cells within 18 h [10]. Mechanisms of cell death included dysregulation of mitochondrial dynamics [11], elevated intracellular calcium, and increased oxidative stress in the form of increased superoxide and nitric oxide levels [12]. *In vivo* studies also reveal RGC death associated with Hhcy (e.g. RGC death in two mouse models of Hhcy, one with deficiencies of cystathionine β-synthase (*Cbs*) [13,14], and the other with deficiencies of methylene tetrahydrofolate reductase (*Mthfr*) [15]). Regarding these models of Hhcy, CBS is a key enzyme in the transsulfuration pathway; it mediates conversion of Hcy to cystathionine, which is then converted to cysteine, a key constituent of the tripeptide glutathione. CBS is present at the gene and protein level throughout the murine retina [13]. MTHFR is a key enzyme in the remethylation pathway; it reduces N_5,N_{10}-methylenetetrahydrofolate to N_5-methyl-tetrahydrofolate, which then donates a methyl group to Hcy to generate methionine (in the presence of vitamin B_{12} and methionine synthase). MTHFR is also present in the mouse retina at both the gene and protein level [15]. Both murine models of Hhcy have approximately 2-fold greater Hcy in retina compared to WT mice [13,15]. The RGC loss *in vivo* is notably mild compared to the rapid death observed in primary cultures of neurons treated with Hcy.

The differential sensitivity of RGCs exposed to Hhcy *in vitro* versus *in vivo* led subsequently to evaluation of the role of retinal Müller cells in buffering the excitotoxic effects of Hhcy [16]. Müller cells are the principle glial cells in retina; they provide trophic and energetic support to adjacent neurons, including RGCs [17,18]. Exposure of cultured primary Müller cells to modest levels of Hhcy actually led to decreased oxidative stress (rather than increased oxidative stress as was observed in RGCs). Decreased levels of reactive oxygen species (ROS) and increased levels of the antioxidant molecule glutathione were detected in primary Müller cells exposed to Hhcy conditions [16]. Thus, in cultured cells there was a differential response between neurons and glia to Hhcy, specifically RGCs versus Müller cells. Molecular analyses of cultured Müller cells exposed to Hhcy revealed increased levels of the major antioxidant transcription factor nuclear factor erythroid 2-related factor 2 (NRF2) and increased levels of several antioxidant molecules whose transcription is regulated by NRF2 [16].

Oxidative stress and mitochondrial dysfunction are major factors in the pathogenesis of neurodegenerative diseases [19] and are implicated in inner retinal neurodegenerative diseases [20,21]. These factors are also mediators of Hhcy-associated neuronal injury [22–26], including Hhcy-induced RGC death [11]. The current study was designed to analyze whether modulation of oxidative stress in Hcy-induced RGC death alters the severity of neuronal loss. To accomplish this, we crossed mice that lack NRF2 (termed *Nrf2*$^{-/-}$ mice) with the two previously characterized models of Hhcy, *Cbs* $^{+/-}$ and *Mthfr* $^{+/-}$ mice, thereby generating *Cbs*$^{+/-}$*Nrf2*$^{-/-}$ and *Mthfr*$^{+/-}$*Nrf2*$^{-/-}$ mice. We performed a series of functional and structural studies of the retina, which revealed reduced visual acuity, inner retinal thickness, and RGC viability in *Cbs*$^{+/-}$*Nrf2*$^{-/-}$ and *Mthfr*$^{+/-}$*Nrf2*$^{-/-}$ mice compared to wildtype (WT).

Given that *Nrf2* expression increases in Hhcy-exposed Müller cells [16], we also investigated its role in protecting RGCs under Hhcy in the current study using an ex-*vivo* indirect co-culture system of primary RGCs and primary Müller cells. We observed a clear viability advantage when RGCs exposed to Hhcy were co-cultured with primary WT Müller cells, whereas *Nrf2*$^{-/-}$ Müller cells did not afford this neuroprotective advantage. Finally, we investigated energy production in the form of mitochondrial and glycolytic functions of Müller cells to account for their neuroprotective properties when exposed to Hhcy. Taken collectively our *in vitro* and *in vivo* results strongly suggest that NRF2 and glial interactions are critical for RGC survival under conditions of elevated Hcy.

Table 1
Number of animals used in the study.

Mouse group	n	Age (months)
Hcy intravitreal injection experiments		
C57BL6/J (wildtype)	10	2–3
SD-OCT analysis of retinal structure		
WT	17	3–4
Nrf2$^{-/-}$	10	3–4
Cbs$^{+/-}$	8	3–4
Cbs$^{+/-}$*Nrf2*$^{-/-}$	9	3–4
Mthfr +/-	8	3–4
Mthfr$^{+/-}$*Nrf2*$^{-/-}$	6	3–4
WT	13	6–7
Nrf2$^{-/-}$	15	6–7
Cbs$^{+/-}$	12	6–7
Cbs$^{+/-}$*Nrf2*$^{-/-}$	10	6–7
Mthfr$^{+/-}$	8	6–7
Mthfr$^{+/-}$*Nrf2*$^{-/-}$	9	6–7
WT	13	10–11
Nrf2$^{-/-}$	16	10–11
Cbs$^{+/-}$	14	10–11
Cbs$^{+/-}$*Nrf2*$^{-/-}$	9	10–11
Mthfr$^{+/-}$	7	10–11
Mthfr$^{+/-}$*Nrf2*$^{-/-}$	7	10–11
ERG: pSTR and nSTR (electrophysiological analysis)		
WT	5	10–11
Nrf2$^{-/-}$	5	10–11
Cbs$^{+/-}$	6	10–11
Cbs$^{+/-}$*Nrf2*$^{-/-}$	5	10–11
Mthfr$^{+/-}$	5	10–11
Mthfr$^{+/-}$*Nrf2*$^{-/-}$	5	10–11
IOP detection		
WT	7	10–11
Nrf2$^{-/-}$	6	10–11
Cbs$^{+/-}$	5	10–11
Cbs$^{+/-}$*Nrf2*$^{-/-}$	5	10–11
Mthfr$^{+/-}$	4	10–11
Mthfr$^{+/-}$*Nrf2*$^{-/-}$	4	10–11
OptoMotry Analysis		
WT	4	10–12
Nrf2$^{-/-}$	3	10–12
Cbs$^{+/-}$	4	10–12
Cbs$^{+/-}$*Nrf2*$^{-/-}$	4	10–12
Mthfr$^{+/-}$	3	10–12
Mthfr$^{+/-}$*Nrf2*$^{-/-}$	3	11–12
GCL cell counting in retinal cryosections		
WT	7	11–12
Nrf2$^{-/-}$	7	11–12
Cbs$^{+/-}$	6	11–12
Cbs$^{+/-}$*Nrf2*$^{-/-}$	6	11–12
Mthfr$^{+/-}$	5	11–12
Mthfr$^{+/-}$*Nrf2*$^{-/-}$	6	11–12
GFAP immunostaining in retinal cryosections		
WT	4	11–12
Nrf2$^{-/-}$	3	11–12
Cbs$^{+/-}$	5	11–12
Cbs$^{+/-}$*Nrf2*$^{-/-}$	4	11–12
Mthfr$^{+/-}$	4	11–12
Mthfr$^{+/-}$*Nrf2*$^{-/-}$	4	11–12

2. Methods and materials

2.1. Animals

The numbers of mice used for experiments in this study are listed in Table 1. Breeding pairs of *Mthfr*$^{+/-}$ mice (Dr. R. Rozen, McGill University, Montreal, Canada), *Cbs*$^{+/-}$ mice (Jackson Laboratories, Bar Harbor, ME, USA), and *Nrf2*$^{-/-}$ mice (Dr. M. Yamamoto, Tohoku University, Sendai, Japan) were used to establish colonies of these strains and to generate *Mthfr*$^{+/-}$*Nrf2*$^{-/-}$ and *Cbs*$^{+/-}$*Nrf2*$^{-/-}$ mice. Confirmation of genotype was performed as described [13,15,27–29]. The *Crb1*$^{rd8/rd8}$ mutation, which causes focal disruption of the retina in

some mouse strains [30], was not detected in any mice used in the study. Breeder C57BL/6J mice (Jackson Laboratories) were used to generate WT controls. Mice were fed Teklad Irradiated Rodent Diet 8904 for breeding or Diet 2918 for maintenance (Teklad, Madison, WI, USA). Animals were subjected to a standard 12-h light: 12-h dark cycle. Maintenance and treatment of animals adhered to institutional guidelines for humane treatment of animals and to the ARVO statement for Use of Animals in Ophthalmic and Vision Research.

To simulate acute exposure to Hhcy, we administered Hcy as a single intravitreal injection following our published method [31]. Briefly, the eyes of deeply anesthetized 8 wk WT mice were gently proposed and 1 μl L-homocysteine thiolactone [2.5 mM] was injected at the limbus using a 33-g needle affixed to a Hamilton syringe (Hamilton, Reno, NV). Assuming intravitreal volume as 25 μL this injection yields a final intravitreal concentration of ~100 μM Hcy [41]. The contralateral eye was injected intravitreally with 1 μl 0.01 M phosphate buffered saline (PBS) and served as a control.

2.2. Evaluation of retinal function and structure

2.2.1. Optical coherence tomography (OCT)

A longitudinal study was performed to evaluate retinal structure *in situ* in mice at 4, 7 and 10 months. An additional group of mice that had received a single intravitreal injection of Hcy were evaluated at ~7 and ~25 days post-injection. Mice were anesthetized with ketamine/xylazine as described [32]. Retinal architecture was assessed *in vivo* using a Bioptigen Spectral Domain Ophthalmic Imaging System (SDOIS; Bioptigen Envisu R2200, NC). The OCT imaging protocol included averaged single B scan and volume intensity scans with images centered on the optic nerve head. Post-imaging analysis included autosegmentation analysis and manual assessment of retinal layers using InVivoVue™ Diver 2.4 software (Bioptigen). We measured total retinal thickness and thicknesses of the nerve fiber layer (NFL), inner plexiform layer (IPL), inner nuclear layer (INL), outer plexiform layer (OPL), and outer nuclear layer (ONL). Each layer thickness was plotted separately; data for a given retinal layer in each group were averaged.

2.2.2. Electroretinography

To assess function of ganglion and amacrine cells, mice were subjected to electroretinography (ERG) to detect positive and negative scotopic threshold responses (pSTR and nSTR). Mice were dark adapted overnight. Each mouse was tested under anesthesia (ketamine 80 mg/kg, xylazine 10 mg/kg) using relatively dim stimuli generated with a blue LED (Lightspeed Technologies, Campbell CA) that was neutral density filtered and defocused. Light from the LED was presented to the eye by 1-mm diameter optic fibers that were placed just in front of the pupils. Signals were acquired by DTL fibers placed gently on the corneas, with a drop of hypromellose to keep eyes moist and enhance electrical contact. These signals were transferred to a Psylab amplifier (Contact Precision Instruments, Cambridge MA), with a gain of 10,000, filtered between 0.3 and 400 Hz, with a notch filter at 60 Hz. The amplified signals were digitized by a National Instruments 6323 data acquisition module (National Instruments, Austin, TX, USA), and read into custom software written in Igor Pro (WaveMetrics, Lake Oswego OR). Stimulus intensity was calibrated in scotopic lumens (ILT1700, International Light Technologies, Peabody MA). An interleaved set of intensities just below and above threshold was presented. Averaged responses were analyzed to obtain pSTRs and nSTRs. These are the amplitudes at 110 and 200 ms following the flash, respectively [33].

2.2.3. Visual acuity assessment

Spatial thresholds for opto-kinetic tracking of sine-wave gratings were measured using a virtual optokinetic system (OptoMotry, CerebralMechanics, Medicine Hat, Alberta, Canada) [34]. Vertical sine-wave gratings moving at 12°/s or gray of the same mean luminance were projected on four computer monitor screens as a virtual cylinder that surrounded an unrestrained mouse standing on a pedestal at the epicenter. The cylinder hub was continually centered between the mouse's eyes to set the spatial frequency (SF) of the grating at the mouse's viewing position as it shifted its position. Gray was projected while the mouse was moving, but when movement ceased, the gray was replaced with the grating. Grating rotation under these circumstances elicited reflexive optokinetic tracking, which was scored via live video using a method of limits procedure with a yes/no criterion. An SF threshold was generated at 100% contrast through each eye separately in the testing session.

2.2.4. Intraocular pressure

The intraocular pressure (IOP) was measured in 10–11 month old WT, *Nrf2*$^{-/-}$, *Cbs*$^{+/-}$, *Cbs*$^{+/-}$*Nrf2*$^{-/-}$, *Mthfr* $^{+/-}$ and *Mthfr*$^{+/-}$*Nrf2*$^{-/-}$ mice, which were anesthetized using inhaled isofluorane (Butler Animal Health Supply, Dublin, OH, USA). The IOP was measured using a handheld tonometer (Tonolab, Icare Laboratory, Finland) positioned at the center of the cornea. Three repeated measurements were taken from each animal for quantification.

2.2.5. Histologic processing of tissue and microscopic analysis

Eyes enucleated from euthanized mice were flash frozen in liquid nitrogen and embedded in optimal cutting temperature compound (OCT, Elkhart, IN). 10 μm thick cryosections were obtained, which were fixed 10 min in 4% paraformaldehyde, blocked with Powerblock (BioGenex, Fremont, CA) for 1 h at room temperature. Sections were incubated with primary antibodies to detect glial fibrillary acidic protein (GFAP), a marker of gliosis, followed by incubation with Alexa Fluor 488 anti-rabbit IgG (Invitrogen). Retinas were examined using a Zeiss Axio Imager D2 microscope equipped with a high-resolution camera and processed using Zeiss Zen23pro software. The fluorescence intensity of GFAP was quantified using the Zen 2 lite software. Additional sections were stained with hematoxylin and eosin (H&E) to allow scanning of retinal tissue for evidence of gross disruption. It is not possible to quantify the number of cells in the ganglion cell layer (GCL) by OCT, therefore we counted the cells in this layer (in a blinded manner) and expressed the data as number of cells per 100 μm retinal length. The measurements were taken at six points along the retina, three adjacent fields on the temporal and nasal sides beginning 200 μm from the optic nerve. The six measurements were averaged per eye to yield the average number of cells per animal and subsequently per mouse group and were expressed as mean ± standard error of the mean (SEM). Additionally, we performed immunolabeling studies to detect RGCs in retinal cryosections using the RGC-specific marker Brn3a. RGC number was determined for the central retina and expressed as RGCs/100 μm retinal length. Antibodies used for immunolabeling are listed in Table 2.

2.3. Cell culture studies

2.3.1. Isolation and culture of mouse Müller cells

Müller glial cells were isolated from WT and *Nrf2*$^{-/-}$ mice (6–7 days old). Müller cell isolation followed our previously published protocol [16,35,36], which is based on the method of Hicks and Cortois [37]. Briefly, eyeballs were enucleated and incubated in serum-free media overnight; they were enzymatically digested with trypsin/collagenase and retinas were dissected from the remaining tissue. Small retinal tissue pieces were incubated in Dulbecco's Modified Eagle Medium (DMEM), containing 1 g/L glucose, 4 mM L glutamine, 25 mM HEPES and 1 mM sodium pyruvate, (Gibco/ThermoFisher Scientific, Waltham, MA, USA) with 10% fetal bovine serum (FBS, Atlanta Biologicals, Flowery Branch, GA), at 37 °C with 5% CO_2. The isolated cells become confluent within 7–10 days and were used at passages 4–5. Cell purity for both WT and *Nrf2*$^{-/-}$ cell is routinely confirmed using the Müller glial cell-specific marker glutamine synthetase, as well as CRALBP and vimentin, which are expressed in Müller cells, as

Table 2
Antibodies used in the study.

Antibody	Supplier	Dilution
Primary antibodies		
Rabbit anti-GFAP (Z0334)	Dako, Carpentaria, CA	1:500
Goat anti-Vimentin (AB1620)	Chemicon Intl., Temecula, CA	1:100
Rabbit anti beta 3 Tubulin (ab18207	Abcam, Cambridge, MA	1:500
Goat anti-Brn3a C20 (SC31984)	Santa Cruz Corp., Santa Cruz CA	1:100
Mouse anti-CRALBP (NB100-74392)	Novus Biologicals, Littleton, CO	1:50
Rabbit anti Glutamine synthetase (FL-373)	Santa Cruz Corp., Santa Cruz CA	1:50
Secondary Antibodies		
Alexa Fluor 488 anti-Rabbit IgG (H + L)	Invitrogen Molecular Probes, NY	1:1000
Alexa Fluor 555 anti-Mouse IgG (H + L	Invitrogen Molecular Probes, NY	1:1000
Alexa Fluor 488 anti-Goat IgG (H + L)	Invitrogen Molecular Probes, NY	1:1000
Alexa Fluor 555 anti-Rabbit IgG (H + L)	Invitrogen Molecular Probes, NY	1:1000

previously described [16]. Antibodies used for immunostaining are listed in Table 2.

2.3.2. Co-culture of primary RGCs with primary Müller cells

The RGC/Müller cell indirect co-culture system was established based on a published neuron-glial co-culture protocol [38]. RGCs were isolated by a two-step immunopanning procedure from WT mice at post-natal days 2–4 following our published methods, which have been described comprehensively [39]. The neuronal origin of the cells was verified using anti-Brn3 and anti-βIII-tubulin antibodies by immunofluorescence. The freshly isolated cells growing in Neurobasal-DMEM-B27 culture medium (containing 5 μg/ml insulin, 1 mM sodium pyruvate, 0.1 mg/ml transferrin, 60 ng/ml progesterone, 16 μg/ml putrescine, 40 ng/ml sodium selenite, 40 ng/ml triiodo-thyronine, 1 mM L-glutamine, 60 μg/ml N-acetyl cysteine, 2% B27, 50 ng/ml BDNF, 10 ng/ml CNTF, 10 ng/ml forskolin, 10 ng/ml bFGF, 0.1 mg/ml BSA) were plated at a density of ~50,000 cells/well on coverslips situated within a 24-well plate [40]. They were incubated 1 h at 37 °C (5% CO_2) after which Müller cells (plated 1 day previously on 0.4 μm pore size-cell culture inserts (Corning International/ThermoFisher Scientific) at a density of 25,000 cells/insert), were suspended within the wells containing the freshly isolated RGCs. In the co-culture set up both cell types were cultured in the Neurobasal-DMEM-B27 medium in which RGCs are routinely cultured.

2.3.3. Hcy treatment of cultured cells

For RGC/Müller cell co-culture studies, L-homocysteine thiolactone hydrochloride (Sigma-Aldrich, St. Louis, MO) was prepared in RGC medium [50 μM]. For studies using only Müller cells, L-homocysteine thiolactone was prepared in DMEM [50 μM] containing 1 g/L glucose, 4 mM L glutamine, 25 mM HEPES and 1 mM sodium pyruvate and 10% FBS.

2.3.4. Assessment of cell survival and cell death

For co-culture experiments, RGC viability in the presence/absence of Müller cells, was determined by incubating cells 30 min in PrestoBlue Viability reagent (ThermoFisher Scientific) following which fluorescence intensity was measured using a plate reader (Molecular Devices, Sunnyvale, CA) (570 nm excitation/590 nm emission). For the co-culture studies involving Hcy, the incidence of RGCs dying by apoptosis was assessed using the ApopTag Fluorescein In Situ Apoptosis Detection Kit (EMD Millipore Corp, Billerica, MA) according to the manufacturer's instructions. The kit is based on the detection of DNA strand breaks through terminal dUTP nick-end labeling (TUNEL) analysis.

2.4. Glycolysis and mitochondrial function assays

Mitochondrial functional assays were performed using the Seahorse XF96-Analyser (Agilent Technologies, Santa Clara, CA) according to the manufacturer's instructions. 10,000 cells/well were seeded in Agilent Seahorse 96-well XF Cell Culture Microplates. The cartridges were hydrated in a non-CO_2 incubator at 37 °C overnight. WT and *Nrf2*$^{-/-}$ Müller cells were treated with Hcy [50 μM] in DMEM for 20 h. After Hcy incubation the cells were washed three times in XF base medium (Agilent Technologies) containing 4 mM L glutamine, 1 mM pyruvate and 10 mM glucose. To allow pH and temperature calibration, the XF Cell Culture Microplates were incubated in a non-CO_2 incubator (37 °C, 45 min). Oligomycin (final well concentration (FWC) 1 μM), Carbonyl cyanide-4 (trifluoromethoxy) phenylhydrazone (FCCP) (FWC 1 μM), rotenone and antimycin A (FWC 0.5 μM) were serially injected into the wells to measure ATP production, maximal respiration and non-mitochondrial respiration, respectively. Compounds were provided as part of the Agilent Technologies XF Cell Mito Stress Test Kit (Catalog # 103015-100). Spare respiratory capacity and proton leak were then determined using these parameters and basal respiration per the manufacturer's instructions.

To assay glycolytic function, cells were glucose-starved in XF assay medium in a CO_2 free incubator at 37 °C for 1 h. Extracellular acidification rates (ECAR) were measured using the Agilent Seahorse XF-96 Analyser by serially injecting glucose (FWC 10 mM), oligomycin (FWC 1 μM) and 2-dexoyglucose (2-DG) (FWC 50 mM) into the wells. The compounds were provided in the XF Glycolysis Stress test kit; Catalog#: 103020-100. Glycolysis, glycolytic capacity, glycolytic reserve and non-glycolytic acidification were calculated according to the manufacturer's instructions. Data were represented in mpH/min.

To normalize the glycolysis and mitochondrial analyses, Müller cell viability was determined using CyQUANT Direct Cell Proliferation Assay (ThermoFisher Scientific) according to the manufacturer's instructions. The fluorescence readings were determined at an excitation wavelength of 485 nm and an emission of 530 nm.

2.5. Data analysis

The data were subjected to statistical analysis using Prism 6 for Windows Version 6.01 statistical analysis software (GraphPad, La Jolla, CA). All values are reported as mean ± SEM. The specific statistical tests used and post-hoc analyses performed are indicated individually for each experiment within the corresponding figure legends. For all analyses $p < 0.05$ was considered statistically significant.

3. Results

3.1. Effects of acute Hhcy exposure assessed using SD-OCT imaging

To investigate the effects of acute exposure to Hhcy on retinal structure *in vivo* we administered 1 μl Hcy [100 μM] intravitreally in one eye of 8 wk old WT mice; the contralateral eye was injected with PBS [0.01 M]. Retinal structure was analyzed by SD-OCT at 6 and 25 days post-injection. B-scans and volume intensity projections are shown for analysis at day 6 (Fig. 1A–C) and day 25 (Fig. 1D–F). At 6 days post-

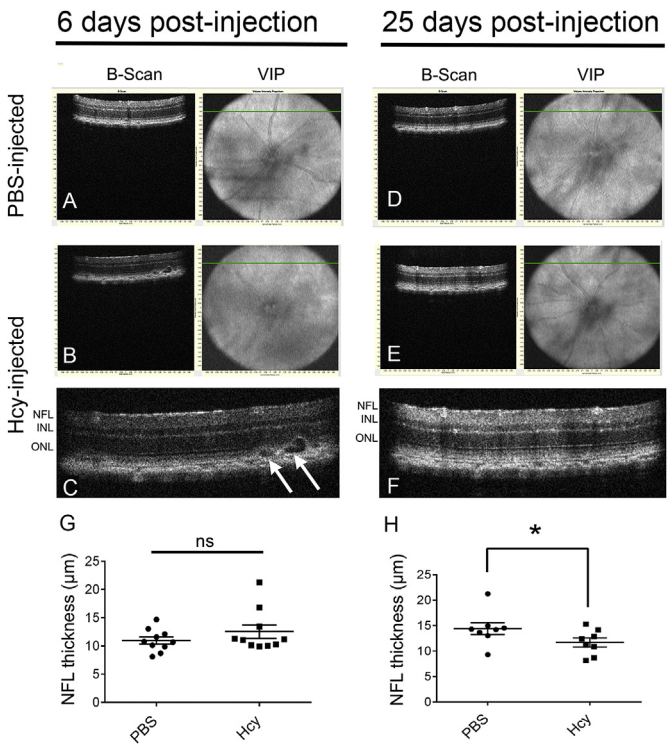

Fig. 1. The nerve fiber layer (NFL) thickness decreases in acute hyperhomocysteinemia. WT mice were injected intravitreally with 100 μM Hcy in one eye and PBS in the contralateral eye at 8 weeks and were subjected to SD-OCT as described in the text. OCT b-scans and volume intensity projections (VIP) were obtained at 6- and 25-days post-injection. PBS-injected eyes (A, D) were normal. Disruption of the outer retina was observed at day 6 in Hcy-injected eyes (B, and enlarged image C, white arrows). The disruption resolved by day 25 post-injection (E, enlarged image F). Quantitative analysis of retinal layer thickness using DIVERs software revealed that only one layer differed between the Hcy- and PBS-injected eyes, which was the NFL at 25-days post-injection (H), though not at 6 days (G). (*$p < 0.05$, Wilcoxon matched-pairs signed rank test.)

Hcy injection focal areas of disruption were detected in the outer retina, characterized by separation of photoreceptor outer segments from underlying RPE (Fig. 1B). These can be best appreciated visualizing a higher magnification B-scan (Fig. 1C). This disruption was observed in 8 of 11 mice in the Hcy-injected eyes, whereas no disruption was observed in PBS-injected eyes (Fig. 1A and D). As this was a longitudinal analysis, we analyzed eyes of the same mice at 25 days post-injection and evaluated the precise areas in which focal disruption had been observed at 6 days. Interestingly, the disruption observed at day 6 (Fig. 1C, arrows) had resolved by day 25 (Fig. 1F), with only one mouse showing mild outer segment-RPE disruption. We leveraged the analytical software (DIVERS) to analyze the thickness of retinal layers following SD-OCT in the mice at 6 and 25 days post-injection. The measurements reflective of the entire retina revealed no significant differences in any retinal layers in the 6 day cohort (Fig. 1G), but a significant decrease in the thickness of the nerve fiber layer (NFL) in the 25 day group (Fig. 1H). The NFL is comprised of axons of RGCs, and the altered thickness is consistent with earlier reports of RGC susceptibility to Hhcy [13,15,30,41,42]. Measurements of the NFL were within normal limits for PBS-injected eyes.

3.2. Absence of NRF2 reduces inner retinal thickness in Hhcy models

Following analysis of consequences of acute Hcy exposure, we explored comprehensively the effects of long-term chronic exposure to Hhcy on retinal structure and function. To accomplish this we studied retinas of *Mthfr* $^{+/-}$ and *Cbs* $^{+/-}$ mice, which have deficiencies in enzymes involved in Hcy metabolism (MTHFR and CBS). Our studies were conducted primarily on mice that were 10–12 months of age, whereas we had previously reported analysis of retina of these mice at ~6 months [13,15]. GCL cell loss and reduced NFL layer thicknesses were reported in these previous studies, suggesting the susceptibility of RGCs to Hhcy. Increased oxidative stress is postulated as a cause of neuronal apoptosis, including RGC death, under Hhcy conditions [11,16]. Owing to the crucial role of NRF2 in protecting retinal neurons under conditions of oxidative stress [43,44] and the previous findings that in retinal Müller cells, Hhcy upregulates the NRF2 antioxidant pathway [16], we crossed the mouse models of Hhcy with *Nrf2*$^{-/-}$ mice to yield animals with chronic Hhcy lacking NRF2. Six mouse groups (WT, *Nrf2*$^{-/-}$, *Cbs*$^{+/-}$, *Cbs*$^{+/-}$*Nrf2*$^{-/-}$, *Mthfr*$^{+/-}$ and *Mthfr*$^{+/-}$*Nrf2*$^{-/-}$) were generated. Longitudinal analysis was performed using SD-OCT to evaluate retinal architecture at 4, 7 and 10–11 months. OCT analyses indicated the most significant changes in retinal layer thicknesses at 10–11 months. Representative OCT B-scans through the optic nerve from 10 to 11 month old mice are shown in Fig. 2 (A-F). There was no evidence of gross retinal disruption in any mouse group; however, quantitation of retinal layer thickness revealed that the IPL was significantly affected in chronic, later-stage Hhcy (Fig. 2G). This layer is comprised of synapses between INL neurons (bipolar and amacrine cells) and cells in the GCL. Significant differences were observed between WT versus *Cbs*$^{+/-}$*Nrf2*$^{-/-}$ and *Mthfr*$^{+/-}$*Nrf2*$^{-/-}$ mice. Whereas WT mice had an IPL thickness of ~42–43 μm, the IPL thickness in the mutants was ~36–37 μm. The data suggest loss of synaptic integrity between inner retinal neurons and cells within the GCL. NFL thickness was reduced in *Cbs*$^{+/-}$*Nrf2*$^{-/-}$ mice (Fig. 2H).

We also examined the combined thickness of the NFL and IPL because it collectively defines the RGC's dendritic arbor (IPL) and axons (NFL). Thinning of these layers is an early biomarker for optic neuropathies including glaucoma [45–50]. *Cbs*$^{+/-}$*Nrf2*$^{-/-}$ and *Mthfr*$^{+/-}$*Nrf2*$^{-/-}$ mice had significantly reduced NFL + IPL thickness compared to WT (Fig. 2I). *Cbs*$^{+/-}$*Nrf2*$^{-/-}$ mice had significantly reduced NFL + IPL compared to *Cbs* $^{+/-}$ mice (Fig. 2I). There were slight differences observed also at 4 months and 7 months (Suppl. Fig. 1). Specifically, at 4 months, the IPL thickness, which typically measures ~47 μm in WT was less than 45 μm in *Cbs*$^{+/-}$/*Nrf2*$^{-/-}$ and *Mthfr* $^{+/-}$ mice; the combined thickness of the IPL and NFL was also significantly reduced in these two groups compared to WT mice. By the time mice had reached 7 months of age, the average IPL thickness in WT was reduced slightly (to ~42–43 μm) and was no longer significantly different from other groups in the study. The only exception to this was the comparison of WT to *Cbs*$^{+/-}$/*Nrf2*$^{-/-}$ mice (Suppl. Fig. 1F). The decrease in IPL and NFL + IPL thickness in the Hhcy mouse models lacking NRF2 suggests that NRF2 plays a crucial role in maintaining RGC health under conditions of Hhcy.

3.3. Absence of NRF2 attenuates visual acuity in Hhcy mouse models

To understand whether decreased IPL and NFL + IPL layers in 10–11 month old *Cbs*$^{+/-}$*Nrf2*$^{-/-}$ and *Mthfr*$^{+/-}$*Nrf2*$^{-/-}$ mice (described in Fig. 2) affected visual function, we examined the optokinetic tracking (OKT) response using the OptoMotry system, which has been utilized in rodents in several studies [34,51,52]. We assessed acuity of the left and right eye of each mouse by measuring the reflexive response for clockwise and counter clockwise movement of gratings with 12°/second drifting speed. Data were recorded as cycles/degree (c/d). WT mice had an average visual acuity of 0.4c/d (Fig. 3). The *Nrf2*$^{-/-}$, *Cbs*$^{+/-}$, and *Mthfr* $^{+/-}$ mice had visual acuity that was similar to WT; however, the Hhcy mice lacking NRF2 (*Cbs*$^{+/-}$*Nrf2*$^{-/-}$ and *Mthfr*$^{+/-}$*Nrf2*$^{-/-}$) had significantly decreased acuity. The *Cbs*$^{+/-}$*Nrf2*$^{-/-}$ mice had an average acuity of ~0.34c/d and the *Mthfr*$^{+/-}$*Nrf2*$^{-/-}$ mice were slightly worse with an average acuity of ~0.30 c/d. In both chronic models of Hhcy, deficiency of NRF2 appeared to reduce visual acuity significantly. The

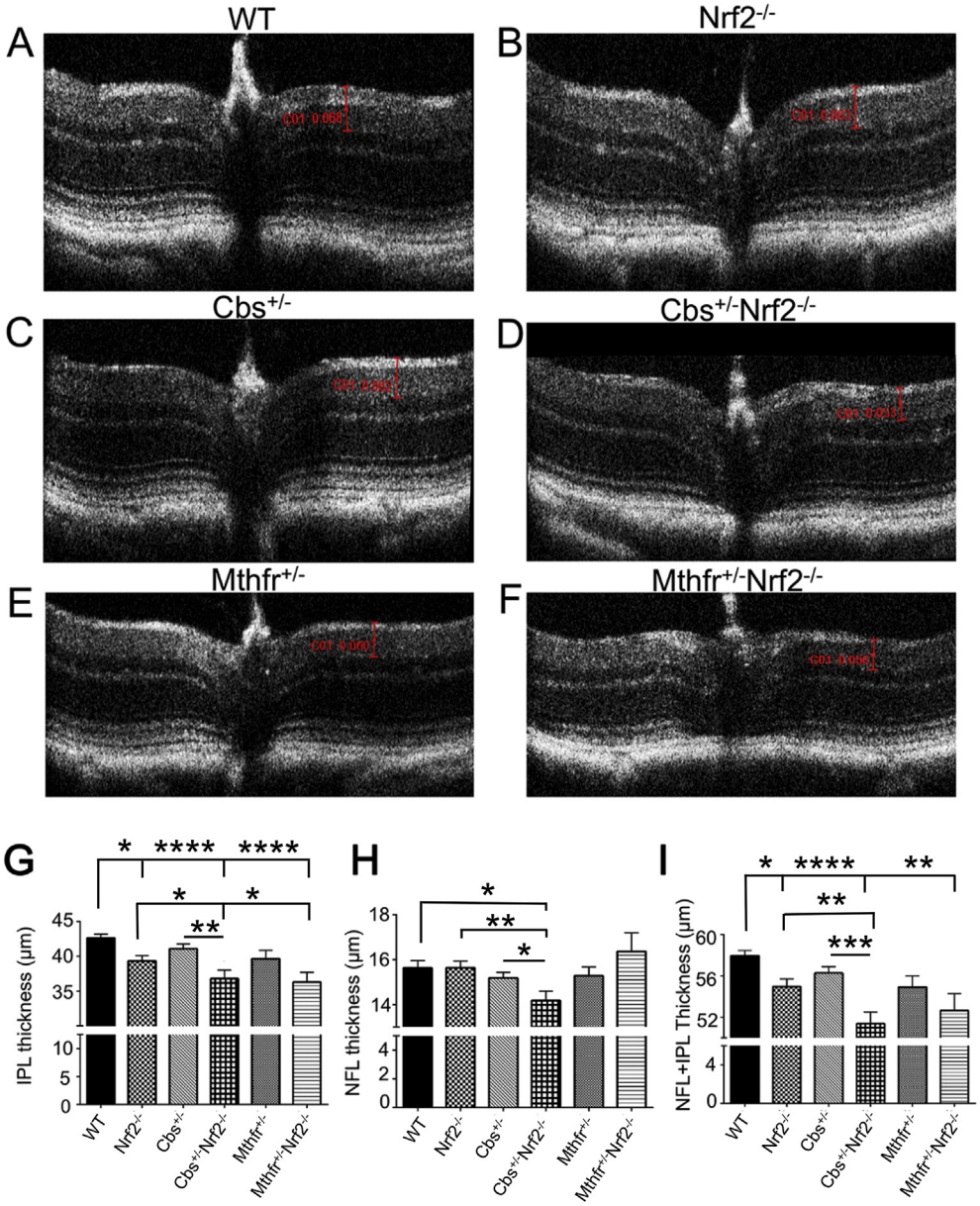

Fig. 2. In the absence of NRF2, the inner plexiform layer (IPL) and nerve fiber layer (NFL) thicknesses decrease in chronic hyperhomocysteinemia. SD-OCT was performed in (A) WT, (B) *Nrf2*$^{-/-}$, (C) *Cbs*$^{+/-}$, (D) *Cbs*$^{+/-}$*Nrf2*$^{-/-}$, (E) *Mthfr* $^{+/-}$ *and* (F) *Mthfr*$^{+/-}$*Nrf2*$^{-/-}$ mice at 10–11 months and representative b-scan images taken through the optic nerve are shown for each mouse group. Retinal layer thicknesses were quantified using DIVERS software. Significant differences in the thickness of the (G) IPL, (H) NFL, (I) IPL-NFL combined were observed compared to WT mice and other mice in the study as indicated (*p < 0.05, **p < 0.01, ****p < 0.0001, One-way ANOVA, Tukey multiple comparison test).

data suggest the important role of NRF2 in offsetting Hhcy-compromised visual function. Interestingly, diminished visual acuity has been reported also in *Nrf2*$^{-/-}$ mice with autoimmune encephalomyelitis [52].

3.4. Absence of NRF2 accelerates the loss of GCL cells in Hhcy mouse models

OCT analysis revealed thinning of IPL and NFL + IPL in *Cbs*$^{+/-}$*Nrf2*$^{-/-}$ and *Mthfr*$^{+/-}$*Nrf2*$^{-/-}$ mice with age (Fig. 2, Suppl. Fig 1). The IPL and NFL are the pre- and trans-synaptic layers, respectively, for RGCs that occupy the GCL. Amacrine cells also occupy this layer. It is not possible to quantify the number of cells in the GCL using OCT, therefore we harvested eyes from 11 to 12 month old mice, prepared them for histology (Fig. 4A) and counted the number of cells in the GCL in H&E-stained cryosections as described [15]. Typically, WT mice have ~13–14 cells per 100 μm retinal length (Fig. 4B). Analysis of the GCL cell number revealed a significant decrease in *Cbs* $^{+/-}$ mice (~10 cells/100 μm length). This GCL loss was exacerbated in the absence of *Nrf2* such that *Cbs*$^{+/-}$*Nrf2*$^{-/-}$ mice had ~8 cells/100 μm retinal length (Fig. 4B). Similarly, *Mthfr*$^{+/-}$*Nrf2*$^{-/-}$ mice had significantly fewer cells compared to WT. There was a trend toward fewer GCL cells in *Mthfr* $^{+/-}$ mice, although the difference did not reach statistical significance (Fig. 4B). Immunolabeling of RGCs using Brn3a confirmed these data (Suppl. Fig. 2). Collectively, the OCT and histological results confirm the sensitivity of RGCs to Hhcy, which is exacerbated by NRF2 deficiency.

The histological observations are supported also by electrophysiological studies performed prior to histologic analysis in 10–11 month old mice in which there were significant differences observed at some intensities. Specifically, we observed significantly decreased pSTR, which reflects RGC function, in the *Cbs* $^{+/-}$ mice compared with WT mice (Suppl. Fig. 3A), although no significant pSTR differences were observed in *Mthfr*$^{+/-}$*Nrf2*$^{-/-}$ or *Cbs*$^{+/-}$*Nrf2*$^{-/-}$ mice (Suppl. Fig. 3B). The nSTR reflects amacrine function. While no significant nSTR differences were observed in *Cbs* $^{+/-}$ mice (Suppl. Fig. 3C), there were significant differences in nSTR in the *Cbs*$^{+/-}$*Nrf2*$^{-/-}$ and *Mthfr*$^{+/-}$*Nrf2*$^{-/-}$ mice compared with WT mice (Suppl. Fig. 3D).

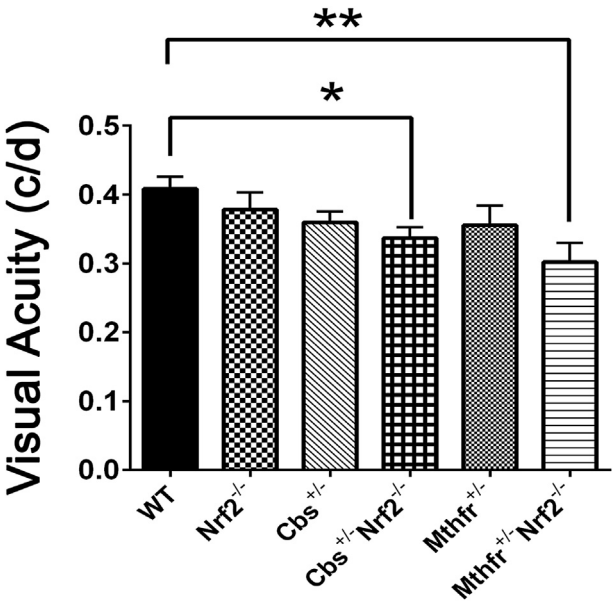

Fig. 3. In the absence of NRF2, visual acuity decreases in chronic hyperhomocysteinemia. Visual acuity threshold, measured as the optokinetic tracking (OKT) response and recorded as cycles/degree (c/d) in WT, *Nrf2*$^{-/-}$, *Cbs*$^{+/-}$, *Cbs*$^{+/-}$*Nrf2*$^{-/-}$, *Mthfr* $^{+/-}$ and *Mthfr*$^{+/-}$*Nrf2*$^{-/-}$ mice at 10–12 months, was performed using the OptoMotry software and apparatus. Significant differences were observed in *Cbs*$^{+/-}$*Nrf2*$^{-/-}$ and *Mthfr*$^{+/-}$*Nrf2*$^{-/-}$ mice compared to WT. (*p < 0.05, **p < 0.01, One-way ANOVA, Tukey multiple comparison test.).

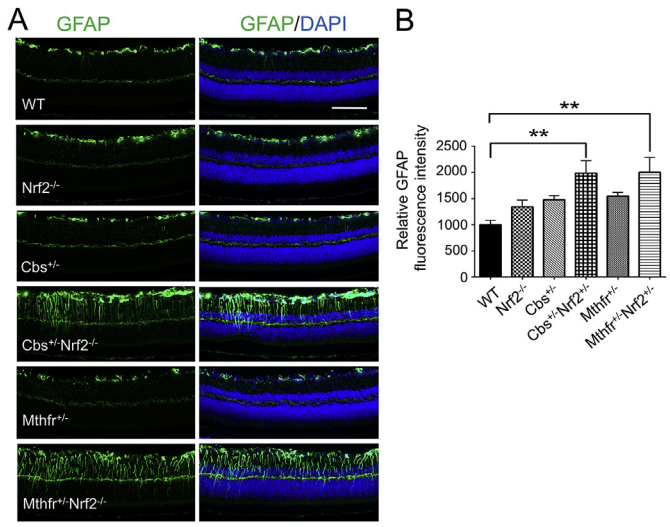

Fig. 5. Deletion of NRF2 exacerbates gliosis in two hyperhomocysteinemic mouse models. (A) Representative photomicrographs of retinal cryosections from *WT, Nrf2*$^{-/-}$, *Cbs*$^{+/-}$, *Cbs*$^{+/-}$*Nrf2*$^{-/-}$, *Mthfr*$^{+/-}$, *Mthfr*$^{+/-}$*Nrf2*$^{-/-}$ mice at 11–12 months that were subjected to immunodetection of glial fibrillary acidic protein (GFAP, green), considered a marker of retinal gliosis and 4′,6-diamidino-2-phenylindole (DAPI, blue), to label cell nuclei (calibration bar = 100 μm). (B) Quantification of immunofluorescent detection of GFAP. (**p < 0.01, One-way ANOVA and Tukey multiple comparison tests.).

3.5. Absence of NRF2 increases GFAP levels in Hhcy mouse models

The reduced thickness of inner retinal layers combined with fewer cells in the GCL observed in Hhcy mice lacking NRF2 (Figs. 1–4) prompted evaluation of the level of GFAP. In the healthy retina, GFAP is detected primarily in retinal astrocytes, which reside in the GCL. In the absence of retinal pathology, there is limited GFAP detected in Müller glial cells; however, under stress Müller cells upregulate GFAP, which is considered a marker of gliosis [53–56]. Increased Müller cell GFAP expression has been reported in Hhcy mouse models [14,15] and in Hcy-exposed primary Müller cells [16]. Here we investigated whether

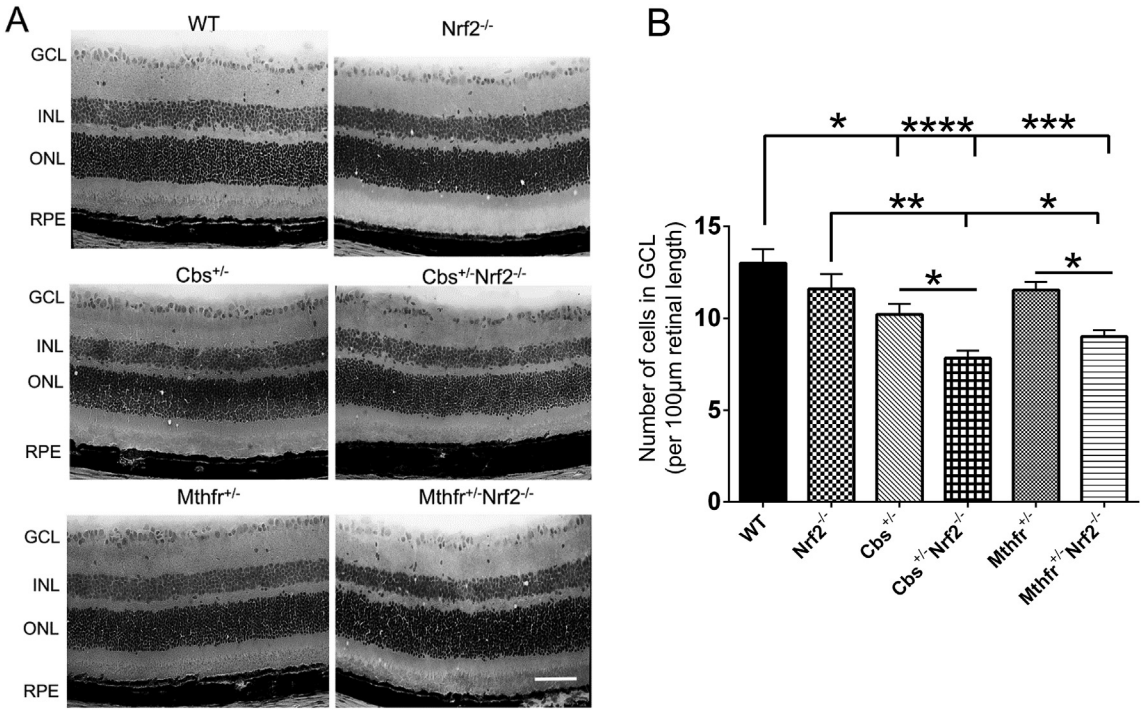

Fig. 4. In the absence of NRF2, there are fewer cells in the ganglion cell layer (GCL) in chronic hyperhomocysteinemic mice. (A) Representative photomicrographs of H&E-stained retinal cryosections images from *WT, Nrf2*$^{-/-}$, *Cbs*$^{+/-}$, *Cbs*$^{+/-}$*Nrf2*$^{-/-}$, *Mthfr*$^{+/-}$, and *Mthfr*$^{+/-}$*Nrf2*$^{-/-}$ mice at 11–12 months. (Calibration bar = 50 μm). (B) Sections were used to quantify the number of cells within the GCL and data were expressed as cell number/100 μm retinal length. (*p < 0.05, ***p < 0.001, ****p < 0.0001, One-way ANOVA, Tukey multiple comparison test.)

absence of NRF2 exacerbates gliosis in Hhcy mouse retinas. Using immunofluorescence we evaluated GFAP levels in retinal cryosections of 11–12 month old WT, *Nrf2*$^{-/-}$, *Cbs*$^{+/-}$, *Cbs*$^{+/-}$*Nrf2*$^{-/-}$, *Mthfr* $^{+/-}$ and *Mthfr*$^{+/-}$*Nrf2*$^{-/-}$ mice (Fig. 5A) and quantified the fluorescence intensity (Fig. 5B). WT and *Nrf2*$^{-/-}$ mice had minimal GFAP levels, and immunofluorescence was limited to the GCL. Radially oriented GFAP labeling, consistent with the radial orientation of Müller cells, was detected in the GCL and IPL of *Cbs* $^{+/-}$ and *Mthfr* $^{+/-}$ mice, although the level of immunofluorescence was not statistically greater than WT. In the retinas of *Cbs*$^{+/-}$*Nrf2*$^{-/-}$ and *Mthfr*$^{+/-}$*Nrf2*$^{-/-}$ mice, GFAP immunofluorescence was considerable in the INL, IPL, GCL (Fig. 5A) and was significantly greater than levels detected in the other mouse groups (Fig. 5B). The data indicate that absence of NRF2 accelerates retinal gliosis in Hhcy mice. Despite the increased gliosis accompanied by RGC death in the Hhcy models lacking NRF2, there was no significant increase in IOP in these animals (*Cbs*$^{+/-}$*Nrf2*$^{-/-}$ and *Mthfr*$^{+/-}$*Nrf2*$^{-/-}$ mice) compared to the other mouse groups (Suppl. Fig. 4).

3.6. Müller glial-specific Nrf2 is critical for RGC survival under conditions of elevated Hcy: in vitro indirect co-culture studies

The increased cell loss in the GCL and thinning of the IPL/NFL in Hhcy models devoid of NRF2 compared to the milder cell loss and IPL/NFL thinning in the genetic Hhcy models in which NRF2 is expressed is consistent with reports implicating increased oxidative stress in Hhcy-linked neuron death [11,16,23,57,58]. In retina, NRF2 is expressed predominantly in Müller glial cells [44]. In previous studies we found that *Nrf2* gene expression, as well as NRF2 protein levels, are increased when Müller cells are exposed to elevated Hcy [16]. Owing to the crucial role Müller glial cells play in protecting the retinal neurons under stressful conditions, we established a neuron-glia indirect co-culture system using primary Müller and primary RGCs to evaluate the relationship of these two cells in managing Hcy-induced stress.

Primary RGCs isolated from postnatal mouse retina were cultured on glass coverslips in a 24 well plate and primary Müller cells growing on a porous transwell insert were placed above the RGCs such that the media in which RGCs were growing was conditioned by the Müller cells as depicted in Fig. 6A. We compared the viability of RGCs grown in the absence or presence of Müller cells and observed substantially more RGCs in the co-culture condition (Fig. 6B and C). After co-culturing with Müller cells for 4 days, RGCs were subjected to immunofluorescence analysis to detect Brn3a and βIII-tubulin, two reliable markers for these cells [59,60]. We observed more Brn3a- and βIII-tubulin-positive cells in RGCs indirectly co-cultured with Müller cells compared to those grown in isolation (Fig. 6B). We evaluated the relative viability of RGCs grown with/without Müller cells and detected significantly more viable cells in the in-direct co-culture condition (Fig. 6C). We next investigated effects of Hhcy on RGC death in the absence/presence of indirect Müller cell co-culture. We treated RGCs with 50 μM Hcy, a concentration that is known to induce significant cell death within 24 h exposure [10,12,16]. Using the TUNEL assay as an indicator of cellular apoptosis, we observed 60% apoptotic cells in primary RGCs (no co-culture) subjected to Hcy treatment (Fig. 6D.1), whereas co-culture with WT Müller cells reduced significantly the incidence of TUNEL-positive RGCs; indeed the value was similar to non-Hcy treated cells (Fig. 6D.2). Interestingly, when Hcy-exposed RGCs were co-cultured with Müller cells harvested from *Nrf2*$^{-/-}$ mice (Fig. 6D.3), RGC survival did not improve. Rather, the incidence of TUNEL-positive cells was similar to Hcy-exposed RGCs without co-culture (Fig. 6E). These data strongly suggest that Müller cells condition the media for RGCs, providing trophic support that attenuates Hcy-induced cell death. The identity of Müller cells in these cultures was confirmed using known Müller cell markers CRALBP, glutamine synthetase (GS) and vimentin (Suppl. Fig. 5).

3.7. Hcy increases the spare respiratory capacity and glycolytic reserve in WT Müller cells, but not in *Nrf2*$^{-/-}$ Müller cells

It is known that excess Hcy levels impair mitochondrial dynamics of RGCs [11]; however, effects of Hcy on Müller cell metabolic function have not been investigated. Müller cells require considerable energy production. We investigated the effect of excess Hcy on cellular respiration (both mitochondrial and glycolytic) in WT Müller cells compared to *Nrf2*$^{-/-}$ Müller cells. We exposed primary WT Müller cells to 50 μM Hcy for 20 h and measured the cellular mitochondrial respiration as oxygen consumption rates (OCR) after sequentially adding oligomycin, FCCP and antimycin A and rotenone to the cells (Fig. 7A). Hcy exposure of Müller cells did not impair mitochondrial function; instead the cells had significantly higher spare respiratory capacity compared to the untreated control cells (Fig. 7B). Spare capacity reflects the capability of cells to respond to an energetic demand, reflecting the cells fitness under stress. These studies were performed also in primary *Nrf2*$^{-/-}$ Müller cells to evaluate the influence of NRF2 on their capacity to mount a beneficial metabolic response to Hhcy. *Nrf2*$^{-/-}$ Müller cells were exposed to 50 μM Hcy for 20 h (Fig. 7C). Assessment of mitochondrial function showed that unlike the WT Müller cells (Fig. 7B), *Nrf2*$^{-/-}$ Müller cells had significantly reduced basal respiration when treated with Hcy and spare capacity remained unaltered by Hcy treatment (Fig. 7C and D). We replotted the data in Fig. 7B and D to allow comparison of mitochondrial function in WT versus *Nrf2*$^{-/-}$ Müller cells exposed to Hcy (Fig. 7E).

Considering the high glycolytic dependency reported in Müller cells [61] and the ability reported in other cell types to increase glycolysis during stressful conditions [62], we analyzed glycolytic function in WT and *Nrf2*$^{-/-}$ Müller cells exposed to 50 μM Hcy for 20 h (Fig. 8A and 8C, respectively). Following the sequential addition of glucose, oligomycin and 2-DG the ECAR values were recorded. We noted that the glycolytic reserve was ~8 mpH/min in WT Müller cells. Interestingly, after cells had been exposed 20 h to 50 μM Hcy, the glycolytic reserve increased significantly (Fig. 8B). The analysis was performed also in primary *Nrf2*$^{-/-}$ Müller cells (Fig. 8C and D). Upon sequential addition of glucose, oligomycin and 2-DG the ECAR values were recorded (Fig. 8C). The increased glycolytic reserve observed in Hcy-treated WT Müller cells (Fig. 8B), was not evident in *Nrf2*$^{-/-}$ Müller cells exposed to excess Hcy (Fig. 8D). We replotted the data in Fig. 8B and D to permit comparison of glycolytic function in WT versus *Nrf2*$^{-/-}$ Müller cells exposed to Hcy (Fig. 8E). As has been reported in other cell types under stress, glycolysis increases significantly in *Nrf2*$^{-/-}$ Müller cells compared with WT. Taken collectively, the data shown in Figs. 7 and 8 suggest that NRF2 plays an important role in Müller cell mitochondrial and glycolytic adaptive responses to Hhcy.

4. Discussion

Hhcy is implicated in several retinal degenerative diseases including glaucoma [1,3,6,63,64] and Hcy levels are elevated in plasma and tears of patients with some forms of the disease, especially XFS [65,66]. RGC loss is the defining cellular event underlying glaucoma, a disease with complex pathogenicity.

It is not surprising that Hcy has been implicated as directly toxic to retinal neurons given that it has excitotoxic properties and has been associated with oxidative stress. The clinical literature, however, has been confusing with respect to Hhcy and glaucoma and it is unclear whether Hcy is merely a biomarker of disease or is actually responsible for cell death [9]. Over the past several years, we have conducted experiments aimed at addressing this issue. Earlier studies demonstrated clear toxicity of Hcy to primary ganglion cells [10], but subsequent experiments performed in Hhcy mouse models (*Cbs* $^{+/-}$ and *Mthfr*$^{+/-}$) yielded only modest loss of RGCs [13–15]. This apparent conundrum suggested that the intact retina is equipped to buffer Hhcy in a manner not present in the isolated neuronal population. We reasoned that a

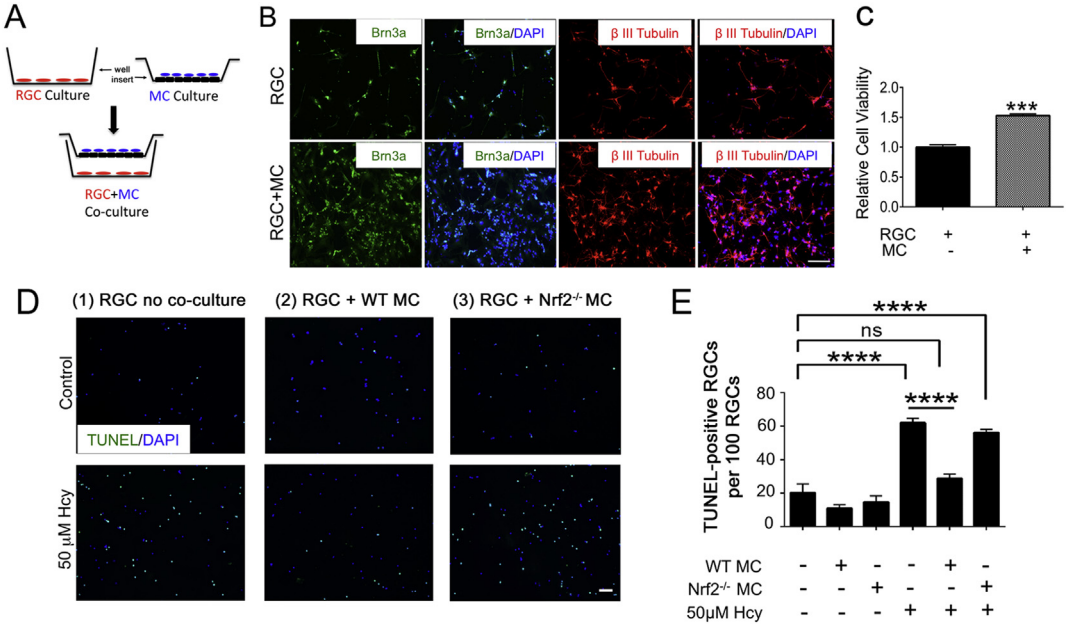

Fig. 6. Evaluation of effects on RGC viability when cells were co-cultured indirectly with Müller cells. (A) Schematic illustration of RGC-Müller glial indirect co-culture. Primary Müller cells (MC) were grown on cell culture inserts (with pore size 0.4 μm) and placed above the primary RGCs, which were growing in culture wells. (B) Immunodetection of RGCs using anti-beta 3 tubulin and anti-Brn3a, two established markers for RGCs. The upper panel reflects RGCs without glial co-culture and the lower panel reflects RGCs indirectly co-cultured with MCs. Calibration bar = 50 μm. (C) Viability of RGCs cultured in the presence or absence of MCs was detected using PrestoBlue and data were quantified (n = 3, ***p < 0.001, Unpaired *t*-test). (D) The effects of Hcy on the incidence of apoptosis in RGCs was determined using the TUNEL assay under three experimental paradigms: (1) RGCs grown without MC co-culture, (2) RGCs grown with WT MC co-culture, (3) RGCs grown with *Nrf2*$^{-/-}$ MC co-culture. DAPI was used to stain cell nuclei. (E) Quantification of TUNEL-positive cells per 100 cells in control and Hcy treated conditions. (*n* = 10, *p < 0.05, ****p < 0.0001, ns p > 0.05, One-way ANOVA, Tukey multiple comparison test.)

likely component of the buffering 'machinery' is the Müller glial cell. In a recent study, we found that unlike RGCs, which manifest increased ROS and decreased viability upon exposure to Hhcy, Müller cells have *decreased* ROS levels and their viability is not compromised [16]. Interestingly, as a response to the Hhcy exposure, Müller cells upregulate *Nrf2* expression and increase the levels of NRF2 protein as well. We postulated that the apparent tempered response to chronic elevation of Hcy in retinas of Hhcy mutant mice might reflect a robust response on the part of Müller cells that likely involved the NRF2 antioxidant response. The current study supports this hypothesis as evidenced by several important findings.

Our first key observation was that acute exposure to Hhcy *in vivo* led to an initial mild disruption of the retinal architecture, which was actually resolved within a few weeks. The powerful analytical tool SD-OCT allowed us to visualize the entire retina, measure individual layers and evaluate integrity in a longitudinal fashion. Even though retinas were mildly disrupted in focal areas 6 days post-injection, the disruptions resolved over a period of ~three weeks. Clearly, there must be mechanisms within the retina that attenuate the response to the acute Hcy insult. To our knowledge, this is the first report of a resolution of the tissues' response to an excitotoxic insult. It is likely that repeated insults, especially if close in time, would not yield such a positive outcome. Importantly, even though the focal disruptions were resolved, the exposure to Hcy had a negative impact on the thickness of the NFL.

Our second key observation was that oxidative stress exacerbated the deleterious effects of chronic Hhcy *in vivo*. We investigated the consequences of chronic Hhcy on retina when the transcription factor NRF2 was absent using *Cbs*$^{+/-}$*Nrf2*$^{-/-}$ and *Mthfr*$^{+/-}$*Nrf2*$^{-/-}$ mice. NRF2 is arguably the master regulator of the antioxidant response as it modulates the expression of more than 500 cytoprotective genes [67]. Our experiments were prompted by the aforementioned observation that NRF2 levels increased in Hhcy-exposed Müller cells and oxidative stress diminished; conversely *Nrf2*$^{-/-}$ Müller cells were much more vulnerable to Hhcy exposure as evidenced by decreased viability and a markedly reduced antioxidant response to Hhcy-induced stress [16]. Our SD-OCT analysis of the *Cbs*$^{+/-}$*Nrf2*$^{-/-}$ and *Mthfr*$^{+/-}$*Nrf2*$^{-/-}$ mice revealed a pronounced decrease in IPL and NFL thickness compared to the other four groups (WT, *Nrf2*$^{-/-}$, *Cbs*$^{+/-}$, *Mthfr*$^{+/-}$). This was most evident at 10–11 months. This same cohort of mice showed a decrease in visual acuity (OKT response) compared to the other four mouse groups measured. The availability of the OptoMotry system has allowed investigators the capability to measure visual function in mice reproducibly. Earlier studies showed that genetic ablation of *Nrf2* exacerbated the visual deficits in an experimental autoimmune uveitis model, emphasizing the key role NRF2 plays in sustaining retinal function under pathologic conditions [52]. The histologic retinal analysis disclosed significant loss of cells in the GCL in *Cbs*$^{+/-}$*Nrf2*$^{-/-}$ and *Mthfr*$^{+/-}$*Nrf2*$^{-/-}$ mice, which was accompanied by a marked increase in the level of GFAP. The cells that were positive for increased GFAP were the radially-oriented Müller cells. It is noteworthy that despite evidence of exacerbated RGC loss and gliosis in Hhcy mice lacking NRF2, there was not an appreciable difference in IOP compared to other mice. The average IOP measured in six different mouse groups was in the range of 10–13 mmHg, which is within normal limits for pressure. In human patients with XFS, there can be considerable IOP fluctuation observed over a 24 h diurnal period [68]. A limitation of our study was that IOP was measured at a single time point, which may not be an accurate reflection of complete profile of pressure in our animals. Future studies should evaluate IOP systematically over a 24 h period. In addition, it would be useful to follow a cohort of animals at more advanced ages. The oldest age evaluated in our study was 10–11 months. Extending the study to mice that are 18–24 months may reveal age-related pressure changes that were not disclosed in the current study.

The findings that genetic ablation of *Nrf2* exacerbates retinal dysfunction in Hhcy mice prompted us to evaluate whether indirect culture of Müller cells with RGCs could buffer neuronal death induced by Hhcy. It is well established that Müller cells play a crucial role in maintaining retinal neurons [56]. However, our co-culture system did not involve

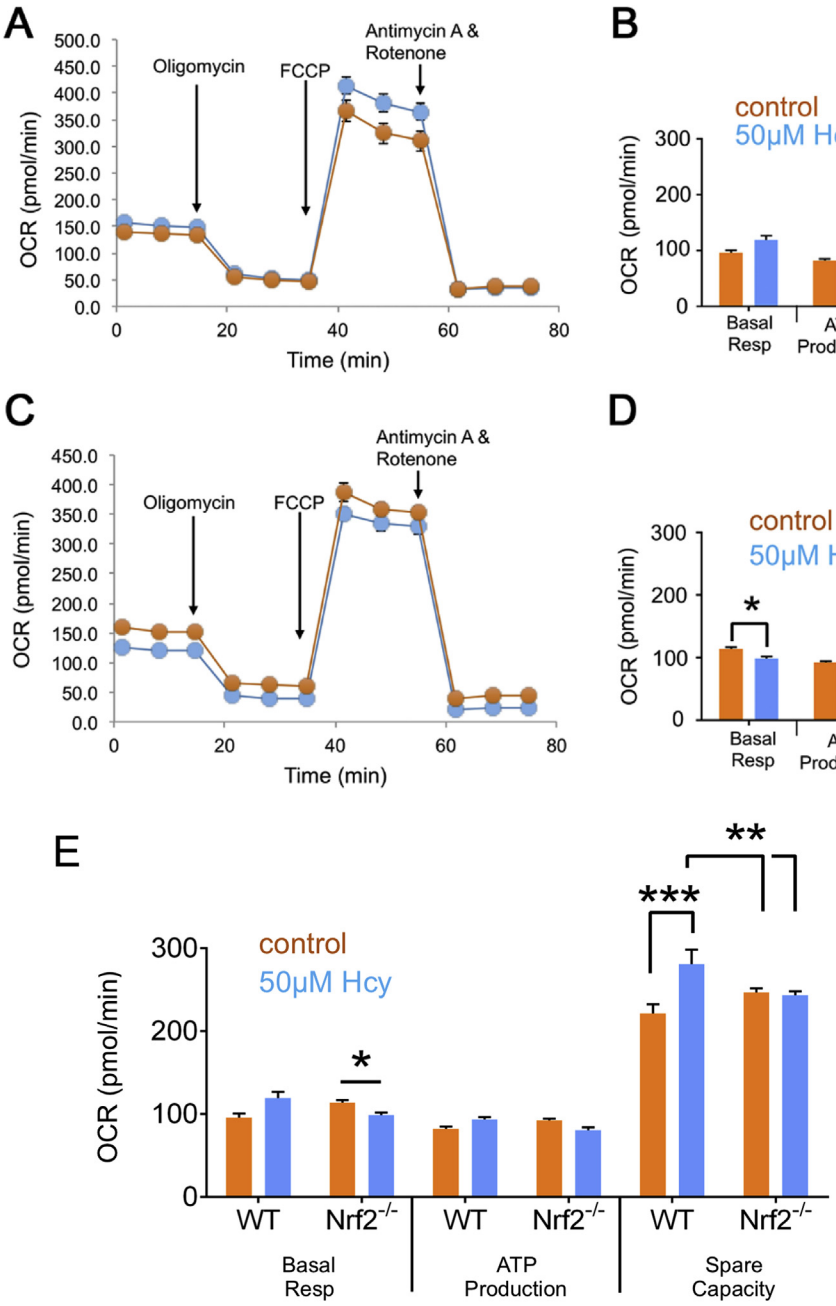

Fig. 7. Analysis of mitochondrial function of WT and *Nrf2*$^{-/-}$ Müller cells treated with homocysteine. Müller cells isolated from WT and *Nrf2*$^{-/-}$ mice were exposed for 20 h to 50 μM Hcy. Mitochondrial function was assessed using the Agilent Seahorse XF Cell Mito Stress Test kit and the Seahorse XF96-Analyser. (A) Mitochondrial respiration in WT non-treated (control) and Hcy-treated cells measured as the oxygen consumption rate (OCR) following exposure to oligomycin, FCCP and antimycin A and rotenone. (B) Quantification of mitochondrial basal respiration (Basal Resp), ATP production and spare respiratory capacity in WT control and Hcy-treated cells. (C) Mitochondrial respiration in *Nrf2*$^{-/-}$ control and Hcy-treated cells measured as OCR. (D) Quantification of mitochondrial basal respiration in *Nrf2*$^{-/-}$ control and Hcy-treated cells. (E) The data in panel B and D were replotted to permit comparison of the WT versus *Nrf2*$^{-/-}$ Müller cells (in the presence/absence of Hcy treatment). The values were normalized to cell viability as measured using the CyQUANT method. (n = 6, *p < 0.05, **p < 0.01,***p < 0.001, Two-way ANOVA, Sidak's multiple comparison test.)

direct cell-cell contact as would occur in the intact retina; rather the Müller cells were seated on a porous filter above the RGCs. The cells were bathed in the same medium, but did not contact each other. Despite this lack of contact, there was a clear benefit to RGCs in being indirectly cultured with the glial cells. Many more RGCs survived under the indirect co-culture conditions compared to RGCs cultured alone. More important was the observation that when the RGCs were treated with Hhcy, there was significantly less cell death in the indirect co-culture with Müller cells than not. The Müller cells that were devoid of NRF2, however, no longer offered this cytoprotective benefit for the RGCs, and cell death with Hhcy exposure was considerable if NRF2 was absent. This is the first evidence of a direct effect for NRF2 in forestalling deleterious effects of Hhcy exposure. We recognize that there may be factors released by Müller cells into the medium that offered significant benefit to the RGCs. It was beyond the scope of the present studies to analyze those factors, but this issue is intriguing and deserving of investigation. Müller cells secrete cytoprotective factors that mitigate neuronal demise, some of which are products of NRF2-targeted upregulation either directly or indirectly. These include catalase, glutathione peroxidase, superoxide dismutase 2, heme oxygenase. In earlier studies, we demonstrated that the genes encoding these proteins are increased in Müller cells exposed to Hhcy [16], however we do not know whether the proteins are secreted by Müller cells in the indirect co-culture system, nor do we know their levels in Hhcy mice.

Müller cells are extraordinarily complex cells and their role in maintaining retinal homeostasis requires that they regulate ion flux (such as K^+ and Ca^{++}), neurotransmitter production, and pH of the retinal milieu [56]. These glial cells are well-studied for their role in taking up and degrading glutamate, which if excessive, is excitotoxic to neurons. Müller cell uptake of glutamate by transporters such as GLAST along with transporters for cystine (cystine-glutamate exchanger) are critical for the synthesis of glutathione. Future studies could investigate these transporters under conditions of Hhcy and determine the level of glutathione in RGC-Müller cell indirect co-culture.

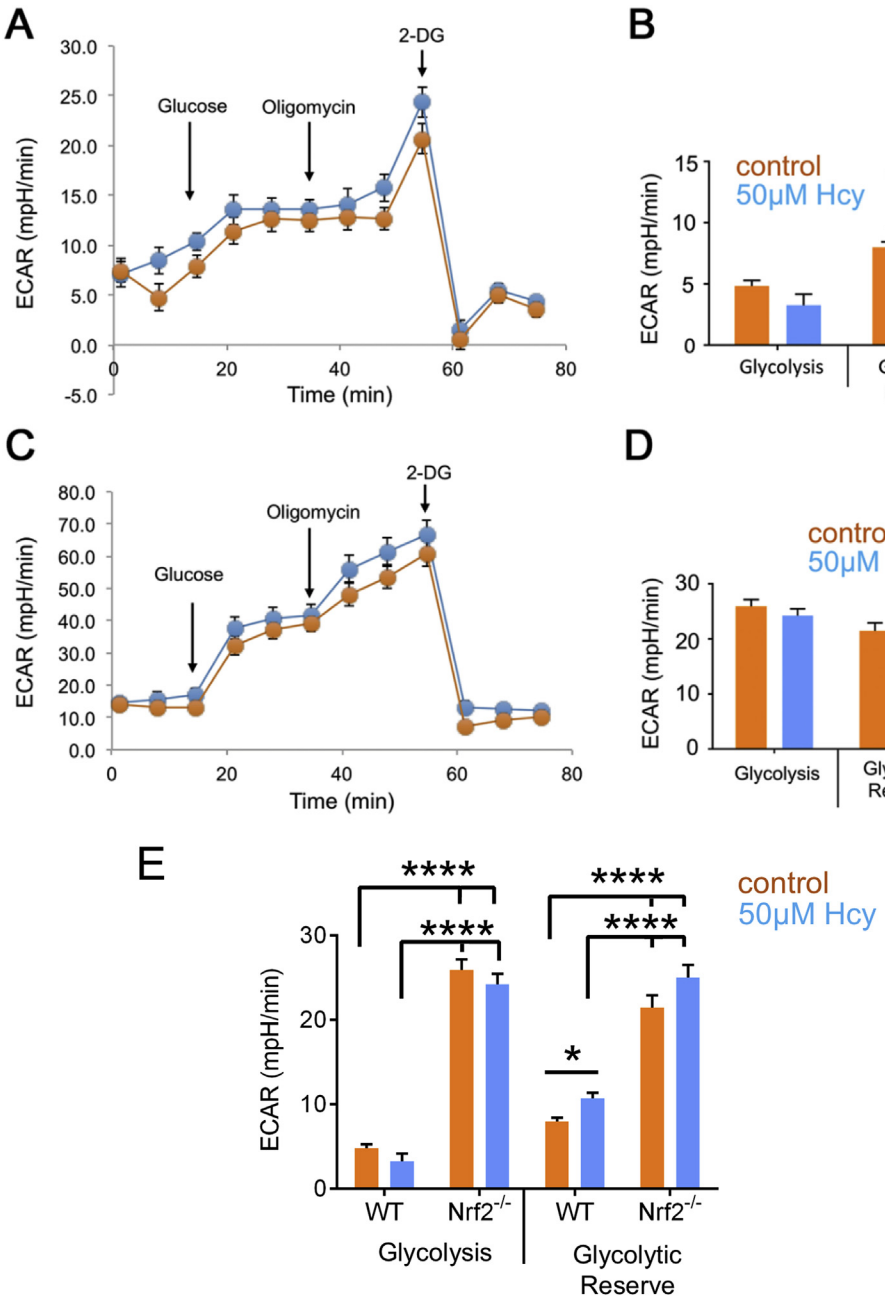

Fig. 8. Analysis of glycolytic function of WT and *Nrf2*$^{-/-}$ Müller cells treated with homocysteine. Müller cells isolated from WT and *Nrf2*$^{-/-}$ mice were exposed 20 h to 50 μM Hcy. Glycolytic function was assessed using the Agilent Seahorse XF Glycolysis Stress Test kit and the XF96 analyser. (A) Glycolytic function in WT non-treated (control) and Hcy-treated cells measured as the extra-cellular acidification rate (ECAR) following exposure to glucose, oligomycin and 2-deoxy-glucose (2-DG). (B) Quantification of glycolysis and glycolytic reserve in WT control and Hcy-treated cells. (C) Glycolytic function in *Nrf2*$^{-/-}$ control and Hcy-treated cells measured as ECAR. (D) Quantification of glycolysis and glycolytic reserve in *Nrf2*$^{-/-}$ control and Hcy-treated cells. (E) The data in panel B and D were replotted to permit comparison of the WT versus *Nrf2*$^{-/-}$ Müller cells (in the presence/absence of Hcy treatment). The values were normalized to cell viability as measured using the CyQUANT method. (n = 6, *p < 0.05, ****p < 0.0001, Two-way ANOVA, Sidak's multiple comparison test.)

Our observations of the benefit of Müller cells in reducing Hcy-induced RGC death raised questions about how Hhcy impacts metabolic functions of these cells. We found that WT Müller cells had robust mitochondrial and glycolytic function. Although glycolysis is considered a major energy source for Müller cells [18], mitochondrial ATP production is also essential for these cells to maintain retinal health [69]. Interestingly, we observed that in WT Müller cells, exposure to excess Hcy did not impair mitochondrial function; rather Hcy-treated WT Müller cells exhibited increased spare respiratory capacity compared to the untreated control cells. Reduced spare respiratory capacity has been linked to neurodegenerative models of excitotoxicity and aging [70–72] and adequate spare capacity is an indicator of healthy mitochondria [73]. Glycolytic function also increased under Hhcy conditions in WT Müller cells as demonstrated by increased glycolytic reserve in Hcy-exposed cells. Glycolytic reserve (like spare capacity) reflects the cells ability to meet additional energy demands. The data suggest mitochondrial and glycolytic adaptations increase in Müller cells to manage the cellular stress induced under Hhcy conditions. This robust mitochondrial and glycolytic response to Hcy exposure evinced by WT Müller cells was completely abrogated in Müller cells isolated from *Nrf2*$^{-/-}$ mice. Previous analysis of mitochondrial function in Hhcy-exposed RGCs revealed alterations of two mitochondrial proteins Opa1 and Fis1 and increased mitochondrial fission [11]. It is technically challenging to subject primary RGCs to mitochondrial analysis using Seahorse technology as performed with Müller cells because the assay requires a confluent monolayer of cells. While this is feasible using primary Müller cells, it is not with primary neurons. Nevertheless, it appears that exposure of RGCs to Hhcy led to dysregulated mitochondrial dynamics, whereas exposure of Müller cells resulted in a positive mitochondrial response.

The current study provides insights on the issue regarding Hhcy as a "disease driver, biomarker or bystander" [9]. First, effects of this excitotoxic amino acid are clearly cell-type dependent. Isolated neurons (at least RGCs) have limited coping mechanisms to manage elevated

Hcy levels, while isolated Müller cells appear to manage Hhcy by increasing their energy production, both mitochondrial and glycolytic. The *in vitro* studies are informative and permit dissection of specific mechanisms. Specifically, they demonstrated the key role that NRF2 plays in the Müller cell's capacity to buffer Hcy. The data support the *in vivo* observations that visual acuity is adversely affected when mice with chronic Hhcy lacked NRF2. The discovery that RGC vulnerability to Hcy may be impacted by the availability of key regulatory molecules, such as NRF2, has implications for retinal degenerative diseases such as glaucoma. With age, NRF2 levels decrease [67] while Hhcy levels increase [74]. Given that glaucoma is a disease associated with increased age, it is quite plausible that under conditions of elevated Hcy and gradually reduced levels of NRF2, the capacity of Müller cells to maintain RGCs is compromised.

Conflicts of interest

The authors declare no conflicts of interest. The funding sponsors had no role in the design of the study; in the collection, analyses or interpretation of data; in the writing of the manuscript; nor in the decision to publish the results. The contents do not represent the views of the U.S. Department of Veterans Affairs or the United States Government.

Acknowledgements

We acknowledge Dr. Masayuki Yamamoto, Tohoku University, Sendai, Japan for his generous gift of the *Nrf2*$^{-/-}$ mice to Dr. B. Thomas and Dr. Rima Rozen for providing breeder pairs of *Mthfr*$^{-/-}$ mice. We acknowledge the EM/Histology Core at Augusta University and Mrs. Penny Roon for excellent assistance with histologic processing of tissue for light microscopic and immunohistochemical studies. We thank Dr. Jennifer Waller, Professor of Population Health Science, Medical College of Georgia for excellent advice and guidance on the statistical analysis of the data. We are grateful to the Medical College of Georgia and to Augusta University for support for instrumentation used in visual function testing performed in this study. A portion of this work is the result of research supported by the use of facilities at the Charlie Norwood VA Medical Center. This work was supported by the National Institutes of Health (R01 EY012830, EY028103, R01 EY027406, R01NS101967), and the James & Jean Culver Vision Discovery Institute of Augusta University.

Appendix A. Supplementary data

Supplementary data to this article can be found online at https://doi.org/10.1016/j.redox.2019.101199.

References

[1] J. Kim, H. Kim, H. Roh, Y. Kwon, Causes of hyperhomocysteinemia and its pathological significance, Arch Pharm. Res. 41 (2018) 372–383.
[2] C. Isobe, T. Murata, C. Sato, Y. Terayama, Increase of total homocysteine concentration in cerebrospinal fluid in patients with Alzheimer's disease and Parkinson's disease, Life Sci. 77 (2005) 1836–1843.
[3] E.A. Ostrakhovitch, S. Tabibzadeh, Homocysteine and age-associated disorders, Ageing Res. Rev. 49 (2019) 144–164.
[4] T.A. Ajith, Ranimenon, Homocysteine in ocular diseases, Clin. Chim. Acta 450 (2015) 316–321.
[5] B. Turgut, M. Kaya, S. Arslan, T. Demir, M. Güler, M.K. Kaya, Levels of circulating homocysteine, vitamin B6, vitamin B12, and folate in different types of open-angle glaucoma, Clin. Interv. Aging 5 (2010) 133–139.
[6] C.I. Clement, I. Goldberg, P.R. Healey, S.L. Graham, Plasma homocysteine, MTHFR gene mutation, and open-angle glaucoma, J. Glaucoma 18 (2009) 73–78.
[7] I.F. Aboobakar, W.M. Johnson, W.D. Stamer, M.A. Hauser, R.R. Allingham, Major review: exfoliation syndrome; advances in disease genetics, molecular biology, and epidemiology, Exp. Eye Res. 154 (2017) 88–103.
[8] R. Ritch, Exfoliation syndrome-the most common identifiable cause of open-angle glaucoma, J. Glaucoma 3 (1994) 176–177.
[9] L.R. Pasquale, T. Borrás, J.H. Fingert, J.L. Wiggs, R. Ritch, Exfoliation syndrome: assembling the puzzle pieces, Acta Ophthalmol. 94 (2016) e505–e512.
[10] Y. Dun, M. Thangaraju, P. Prasad, V. Ganapathy, S.B. Smith, Prevention of excitotoxicity in primary retinal ganglion cells by (+)-pentazocine, a sigma receptor-1 specific ligand, Invest. Ophthalmol. Vis. Sci. 48 (2007) 4785–4794.
[11] P.S. Ganapathy, R.L. Perry, A. Tawfik, R.M. Smith, E. Perry, P. Roon, B.R. Bozard, Y. Ha, S.B. Smith, Homocysteine-mediated modulation of mitochondrial dynamics in retinal ganglion cells, Invest. Ophthalmol. Vis. Sci. 52 (2011) 5551–5558.
[12] P.S. Ganapathy, R.E. White, Y. Ha, B.R. Bozard, P.L. McNeil, R.W. Caldwell, S. Kumar, S.M. Black, S.B. Smith, The role of N-methyl-D-aspartate receptor activation in homocysteine-induced death of retinal ganglion cells, Invest. Ophthalmol. Vis. Sci. 52 (2011) 5515–5524.
[13] P.S. Ganapathy, B. Moister, P. Roon, B.A. Mysona, J. Duplantier, Y. Dun, T.K. Moister, M.J. Farley, P.D. Prasad, K. Liu, S.B. Smith, Endogenous elevation of homocysteine induces retinal neuron death in the cystathionine-beta-synthase mutant mouse, Invest. Ophthalmol. Vis. Sci. 50 (2009) 4460–4470.
[14] A. Tawfik, S. Markand, M. Al-Shabrawey, J.N. Mayo, J. Reynolds, S.E. Bearden, V. Ganapathy, S.B. Smith, Alterations of retinal vasculature in cystathionine-β-synthase heterozygous mice: a model of mild to moderate hyperhomocysteinemia, Am. J. Pathol. 184 (2014) 2573–2585.
[15] S. Markand, A. Saul, P. Roon, P. Prasad, P. Martin, R. Rozen, V. Ganapathy, S.B. Smith, Retinal ganglion cell loss and mild vasculopathy in methylene tetrahydrofolate reductase (Mthfr)-Deficient mice: a model of mild hyperhomocysteinemia, Invest. Ophthalmol. Vis. Sci. 56 (2015) 2684–2695.
[16] S. Navneet, X. Cui, J. Zhao, J. Wang, N.A. Kaidery, B. Thomas, K.E. Bollinger, Y. Yoon, S.B. Smith, Excess homocysteine upregulates the NRF2-antioxidant pathway in retinal Müller glial cells, Exp. Eye Res. 178 (2019) 228–237.
[17] A. Bringmann, I. Iandiev, T. Pannicke, A. Wurm, M. Hollborn, P. Wiedemann, N.N. Osborne, A. Reichenbach, Cellular signaling and factors involved in Müller cell gliosis: neuroprotective and detrimental effects, Prog. Retin. Eye Res. 28 (2009) 423–451.
[18] E. Vecino, F.D. Rodriguez, N. Ruzafa, X. Pereiro, S.C. Sharma, Glia-neuron interactions in the mammalian retina, Prog. Retin. Eye Res. 51 (2016) 1–40.
[19] C. Guo, L. Sun, X. Chen, D. Zhang, Oxidative stress, mitochondrial damage and neurodegenerative diseases, Neural Regen Res. 8 (2013) 2003–2014.
[20] V. Chrysostomou, F. Rezania, I.A. Trounce, J.G. Crowston, Oxidative stress and mitochondrial dysfunction in glaucoma, Curr. Opin. Pharmacol. 13 (2013) 12–15.
[21] E.M. McElnea, B. Quill, N.G. Docherty, M. Irnaten, W.F. Siah, A.F. Clark, C.J. O'Brien, D.M. Wallace, Oxidative stress, mitochondrial dysfunction and calcium overload in human lamina cribrosa cells from glaucoma donors, Mol. Vis. 17 (2011) 1182–1191.
[22] M. Kumar, R.S. Ray, R. Sandhir, Hydrogen sulfide attenuates homocysteine-induced neurotoxicity by preventing mitochondrial dysfunctions and oxidative damage: in vitro and in vivo studies, Neurochem. Int. 120 (2018) 87–98.
[23] N. Bhattacharjee, A. Borah, Oxidative stress and mitochondrial dysfunction are the underlying events of dopaminergic neurodegeneration in homocysteine rat model of Parkinson's disease, Neurochem. Int. 101 (2016) 48–55.
[24] Y. Hirashima, S. Seshimo, Y. Fujiki, M. Okabe, K. Nishiyama, M. Matsumoto, H. Kanouchi, T. Oka, Homocysteine and copper induce cellular apoptosis via caspase activation and nuclear translocation of apoptosis-inducing factor in neuronal cell line SH-SY5Y, Neurosci. Res. 67 (2010) 300–306.
[25] W. Duan, B. Ladenheim, R.G. Cutler, I.I. Kruman, J.L. Cadet, M.P. Mattson, Dietary folate deficiency and elevated homocysteine levels endanger dopaminergic neurons in models of Parkinson's disease, J. Neurochem. 80 (2002) 101–110.
[26] P.A. Abushik, M. Niittykoski, R. Giniatullina, A. Shakirzyanova, G. Bart, D. Fayuk, D.A. Sibarov, S.M. Antonov, R. Giniatullin, The role of NMDA and mGluR5 receptors in calcium mobilization and neurotoxicity of homocysteine in trigeminal and cortical neurons and glial cells, J. Neurochem. 129 (2014) 264–274.
[27] X. Cui, S. Navneet, J. Wang, P. Roon, W. Chen, M. Xian, S.B. Smith, Analysis of MTHFR, CBS, glutathione, taurine, and hydrogen sulfide levels in retinas of hyperhomocysteinemic mice, Invest. Ophthalmol. Vis. Sci. 58 (2017) 1954–1963.
[28] N.A. Kaidery, R. Banerjee, L. Yang, N.A. Smirnova, D.M. Hushpulian, K.T. Liby, C.R. Williams, M. Yamamoto, T.W. Kensler, R.R. Ratan, M.B. Sporn, M.F. Beal, I.G. Gazaryan, B. Thomas, Targeting Nrf2-mediated gene transcription by extremely potent synthetic triterpenoids attenuate dopaminergic neurotoxicity in the MPTP mouse model of Parkinson's disease, Antioxidants Redox Signal. 18 (2013) 139–157.
[29] S. Markand, A. Saul, A. Tawfik, X. Cui, R. Rozen, S.B. Smith, Mthfr as a modifier of the retinal phenotype of Crb1(rd8/rd8) mice, Exp. Eye Res. 145 (2016) 164–172.
[30] B. Chang, R. Hurd, J. Wang, P. Nishina, Survey of common eye diseases in laboratory mouse strains, Invest. Ophthalmol. Vis. Sci. 54 (2013) 4974–4981.
[31] J. Zhao, B.A. Mysona, A. Qureshi, L. Kim, T. Fields, G.B. Gonsalvez, S.B. Smith, K.E. Bollinger, (+)-Pentazocine reduces NMDA-induced murine retinal ganglion cell death through a σR1-dependent mechanism, Invest. Ophthalmol. Vis. Sci. 57 (2016) 453–461.
[32] J. Wang, A. Saul, P. Roon, S.B. Smith, Activation of the molecular chaperone, sigma 1 receptor, preserves cone function in a murine model of inherited retinal degeneration, Proc. Natl. Acad. Sci. U. S. A. 113 (2016) E3764–E3772.
[33] S.M. Saszik, J.G. Robson, L.J. Frishman, The scotopic threshold response of the dark-adapted electroretinogram of the mouse, J. Physiol. 543 (2002) 899–916.
[34] G.T. Prusky, N.M. Alam, S. Beekman, R.M. Douglas, Rapid quantification of adult and developing mouse spatial vision using a virtual optomotor system, Invest. Ophthalmol. Vis. Sci. 45 (2004) 4611–4616.
[35] B. Mysona, Y. Dun, J. Duplantier, V. Ganapathy, S.B. Smith, Effects of hyperglycemia and oxidative stress on the glutamate transporters GLAST and system xc- in mouse retinal Müller glial cells, Cell Tissue Res. 335 (2009) 477–488.
[36] J. Wang, A. Shanmugam, S. Markand, E. Zorrilla, V. Ganapathy, S.B. Smith, Sigma 1

receptor regulates the oxidative stress response in primary retinal Müller glial cells via NRF2 signaling and system xc(-), the Na(+)-independent glutamate-cystine exchanger, Free Radic. Biol. Med. 86 (2015) 25–36.
[37] D. Hicks, Y. Courtois, The growth and behaviour of rat retinal Müller cells in vitro. 1. An improved method for isolation and culture, Exp. Eye Res. 51 (1990) 119–129.
[38] C. Gottschling, E. Dzyubenko, M. Geissler, A. Faissner, The indirect neuron-astrocyte coculture assay: an in vitro set-up for the detailed investigation of neuron-glia interactions, J. Vis. Exp. 117 (2016).
[39] Y. Dun, B. Mysona, T. Van Ells, L. Amarnath, M.S. Ola, V. Ganapathy, S.B. Smith, Expression of the cystine-glutamate exchanger (xc-) in retinal ganglion cells and regulation by nitric oxide and oxidative stress, Cell Tissue Res. 324 (2006) 189–202.
[40] A. Winzeler, J.T. Wang, Purification and culture of retinal ganglion cells from rodents, Cold Spring Harb. Protoc. (2013) 643–652.
[41] P. Moore, A. El-sherbeny, P. Roon, P.V. Schoenlein, V. Ganapathy, S.B. Smith, Apoptotic cell death in the mouse retinal ganglion cell layer is induced in vivo by the excitatory amino acid homocysteine, Exp. Eye Res. 73 (2001) 45–57.
[42] J.S. Kim, Y.K. Kim, S.U. Baek, A. Ha, Y.W. Kim, J.W. Jeoung, K.H. Park, Topographic correlation between macular superficial microvessel density and ganglion cell-inner plexiform layer thickness in glaucoma-suspect and early normal-tension glaucoma, Br. J. Ophthalmol. (2019 Apr 2), https://doi.org/10.1136/bjophthalmol-2018-313732 pii: bjophthalmol-2018–313732. [Epub ahead of print].
[43] N. Himori, K. Yamamoto, K. Maruyama, M. Ryu, K. Taguchi, M. Yamamoto, T. Nakazawa, Critical role of Nrf2 in oxidative stress-induced retinal ganglion cell death, J. Neurochem. 127 (2013) 669–680.
[44] Z. Xu, H. Cho, M.J. Hartsock, K.L. Mitchell, J. Gong, L. Wu, Y. Wei, S. Wang, R.K. Thimmulappa, M.B. Sporn, S. Biswal, D.S. Welsbie, E.J. Duh, Neuroprotective role of Nrf2 for retinal ganglion cells in ischemia-reperfusion, J. Neurochem. 133 (2015) 233–241.
[45] M.J. Kupersmith, M.K. Garvin, J.K. Wang, M. Durbin, R. Kardon, Retinal ganglion cell layer thinning within one month of presentation for optic neuritis, Mult. Scler. 22 (2016) 641–648.
[46] J.Y. Lee, J.M. Kim, I.T. Kim, C.K. Yoo, Y.S. Won, J.H. Kim, H.S. Kwon, K.H. Park, Relationship between plasma homocysteine level and glaucomatous retinal nerve fiber layer defect, Curr. Eye Res. 42 (2017) 918–923.
[47] J.C. Mwanza, M.K. Durbin, D.L. Budenz, F.E. Sayyad, R.T. Chang, A. Neelakantan, D.G. Godfrey, R. Carter, A.S. Crandall, Glaucoma diagnostic accuracy of ganglion cell-inner plexiform layer thickness: comparison with nerve fiber layer and optic nerve head, Ophthalmology 119 (2012) 1151–1158.
[48] V.T. Koh, Y.C. Tham, C.Y. Cheung, W.L. Wong, M. Baskaran, S.M. Saw, T.Y. Wong, T. Aung, Determinants of ganglion cell-inner plexiform layer thickness measured by high-definition optical coherence tomography, Invest. Ophthalmol. Vis. Sci. 53 (2012) 5853–5859.
[49] H.B. Lim, M.W. Lee, J.H. Park, K.M. Kim, Y.J. Jo, J.Y. Kim, Changes in ganglion cell-inner plexiform layer thickness and retinal microvasculature in hypertension: an OCT angiography study, Am. J. Ophthalmol. 199 (2019) 167–176.
[50] E. Kan, K. Yakar, M.D. Demirag, M. Gok, Macular ganglion cell-inner plexiform layer thickness for detection of early retinal toxicity of hydroxychloroquine, Int. Ophthalmol. 38 (2018) 1635–1640.
[51] W. Xiong, A.E. MacColl Garfinkel, Y. Li, L.I. Benowitz, C.L. Cepko, NRF2 promotes neuronal survival in neurodegeneration and acute nerve damage, J. Clin. Investig. 125 (2015) 1433–1445.
[52] C.M. Larabee, S. Desai, A. Agasing, C. Georgescu, J.D. Wren, R.C. Axtell, S.M. Plafker, Loss of Nrf2 exacerbates the visual deficits and optic neuritis elicited by experimental autoimmune encephalomyelitis, Mol. Vis. 22 (2016) 1503–1513.
[53] A.J. Eisenfeld, A.H. Bunt-Milam, P.V. Sarthy, Müller cell expression of glial fibrillary acidic protein after genetic and experimental photoreceptor degeneration in the rat retina, Invest. Ophthalmol. Vis. Sci. 25 (1984) 1321–1328.
[54] M.A. Dyer, C.L. Cepko, Control of Müller glial cell proliferation and activation following retinal injury, Nat. Neurosci. 3 (2000) 873–880.
[55] K.H. Wu, M.C. Madigan, F.A. Billson, P.L. Penfold, Differential expression of GFAP in early v late AMD: a quantitative analysis, Br. J. Ophthalmol. 87 (2003) 1159–1166.
[56] A. Bringmann, T. Pannicke, J. Grosche, M. Francke, P. Wiedemann, S.N. Skatchkov, N.N. Osborne, A. Reichenbach, Müller cells in the healthy and diseased retina, Prog. Retin. Eye Res. 25 (2006) 397–424.
[57] P.I. Ho, S.C. Collins, S. Dhitavat, D. Ortiz, D. Ashline, E. Rogers, T.B. Shea, Homocysteine potentiates beta-amyloid neurotoxicity: role of oxidative stress, J. Neurochem. 78 (2001) 249–253.
[58] M.P. Mattson, T.B. Shea, Folate and homocysteine metabolism in neural plasticity and neurodegenerative disorders, Trends Neurosci. 26 (2003) 137–146.
[59] S.M. Jiang, L.P. Zeng, J.H. Zeng, L. Tang, X.M. Chen, X. Wei, β-III-Tubulin: a reliable marker for retinal ganglion cell labeling in experimental models of glaucoma, Int. J. Ophthalmol. 8 (2015) 643–652.
[60] F.M. Nadal-Nicolás, M. Jiménez-López, P. Sobrado-Calvo, L. Nieto-López, I. Cánovas-Martínez, M. Salinas-Navarro, M. Vidal-Sanz, M. Agudo, Brn3a as a marker of retinal ganglion cells: qualitative and quantitative time course studies in naive and optic nerve-injured retinas, Invest. Ophthalmol. Vis. Sci. 50 (2009) 3860–3868.
[61] B.S. Winkler, M.J. Arnold, M.A. Brassell, D.G. Puro, Energy metabolism in human retinal Müller cells, Invest. Ophthalmol. Vis. Sci. 41 (2000) 3183–3190.
[62] D.Y. Shi, F.Z. Xie, C. Zhai, J.S. Stern, Y. Liu, S.L. Liu, The role of cellular oxidative stress in regulating glycolysis energy metabolism in hepatoma cells, Mol. Canc. 8 (2009) 32.
[63] R.M. Vessani, R. Ritch, J.M. Liebmann, M. Jofe, Plasma homocysteine is elevated in patients with exfoliation syndrome, Am. J. Ophthalmol. 136 (2003) 41–46.
[64] I. Leibovitch, S. Kurtz, G. Shemesh, M. Goldstein, B.A. Sela, M. Lazar, A. Loewenstein, Hyperhomocystinemia in pseudoexfoliation glaucoma, J. Glaucoma 12 (2003) 36–39.
[65] J.B. Roedl, S. Bleich, U. Reulbach, R. Rejdak, J. Kornhuber, F.E. Kruse, U. Schlötzer-Schrehardt, A.G. Jünemann, Homocysteine in tear fluid of patients with pseudoexfoliation glaucoma, J. Glaucoma 16 (2007) 234–239.
[66] S. Bleich, J. Roedl, N. Von Ahsen, U. Schlötzer-Schrehardt, U. Reulbach, G. Beck, F.E. Kruse, G.O. Naumann, J. Kornhuber, A.G. Jünemann, Elevated homocysteine levels in aqueous humor of patients with pseudoexfoliation glaucoma, Am. J. Ophthalmol. 138 (2004) 162–164.
[67] C.J. Schmidlin, M.B. Dodson, L. Madhavan, D.D. Zhang, Redox regulation by NRF2 in aging and disease, Free Radic. Biol. Med. (2019 Jan 14), https://doi.org/10.1016/j.freeradbiomed.2019.01.016 pii: S0891-5849(18)32591-7. [Epub ahead of print].
[68] P. Puska, E. Vesti, G. Tomita, K. Ishida, C. Raitta, Optic disc changes in normotensive persons with unilateral exfoliation syndrome: a 3-year follow-up study, Graefes Arch. Clin. Exp. Ophthalmol. 237 (1999) 457–462.
[69] A.K. Toft-Kehler, D.M. Skytt, A. Svare, E. Lefevere, I. Van Hove, L. Moons, H.S. Waagepetersen, M. Kolko, Mitochondrial function in Müller cells - does it matter? Mitochondrion 36 (2017) 43–51.
[70] N. Yadava, D.G. Nicholls, Spare respiratory capacity rather than oxidative stress regulates glutamate excitotoxicity after partial respiratory inhibition of mitochondrial complex I with rotenone, J. Neurosci. 27 (2007) 7310–7317.
[71] D.G. Nicholls, Spare respiratory capacity, oxidative stress and excitotoxicity, Biochem. Soc. Trans. 37 (2009) 1385–1388.
[72] C. Desler, T.L. Hansen, J.B. Frederiksen, M.L. Marcker, K.K. Singh, L. Juel Rasmussen, Is there a link between mitochondrial reserve respiratory capacity and aging? J. Aging Res. (2012) 192503.
[73] B.G. Hill, G.A. Benavides, J.R. Lancaster Jr., S. Ballinger, L. Dell'Italia, Z. Jianhua, V.M. Darley-Usmar, Integration of cellular bioenergetics with mitochondrial quality control and autophagy, Biol. Chem. 393 (2012) 1485–1512.
[74] W. Herrmann, Significance of hyperhomocysteinemia, Clin. Lab. 52 (2006) 367–374.